Supporting Information

Revealing critical roles of active layer morphology for suppressing interface-related degradation of organic solar cells under illumination

*Yujie Xu,[a] Hao Wang,[b] Yang Liu,[c] Mengfei Xiao,[a] Min Li,[a] Ming Sun,[a] Chen Wang,[a] Wenjun Lu,[a] Xinxin Xia, *[b] Hang Yin,[a] Wei Qin,[a] Maojie Zhang,*[b] Youyu Jiang,*[c] Yinhua Zhou,[c] Xiaotao Hao*[ad] and Xiaoyan Du*[a]*

[a] *School of Physics, State Key Laboratory of Crystal Materials, Shandong University, Jinan 250100, China*

[b] *National Engineering Research Center for Colloidal Materials, School of Chemistry & Chemical Engineering, Shandong University, Jinan 250100, China*

[c] *Wuhan National Laboratory for Optoelectronics, Huazhong University of Science and Technology, Wuhan 430074, China*

[d] *ARC Centre of Excellence in Exciton Science, School of Chemistry, The University of Melbourne, Parkville 3010, Australia.*

Materials

All commercial materials were used without further purification. The indium tin oxide (ITO) glass substrates with a sheet resistance of 15 Ω square^{-1} were acquired from Liaoning Youxuan New Energy Science & Technology Company Limited. PM6, D18, Y6, L8-BO and BTP-eC9 were purchased from Solarmer Materials (Beijing) Inc. Zinc acetate dihydrate and molybdenum trioxide (MoO_3) were purchased from Alfa Aesar. PEDOT:PSS (Clevios PVP Al 4083) was purchased

from Xi'an Polymer Light Technology Corp. PEDOT:F was provided by Professor Zhou Yinhua's research group at the Wuhan Optoelectronics National Laboratory of Huazhong University of Science and Technology, and the solution needed to be filtered before use. All reagents and solvents including ethanolamine, 2-methoxyethanol, chloroform (CF), chlorobenzene (CB), o-Xylene, FS-30 and 1,8-Diiodooctane (DIO) were purchased from Sigma Aldrich.

Device fabrication and characterization

Preparation of the ZnO with sol-gel process

Zinc acetate dihydrate was dissolved in 2-methoxyethanol with addition of ethanolamine forming a homogeneous, colorless and transparent precursor sol. The precursor was keep stirring at room temperature overnight.

Preparation of the solutions

The PM6:Y6 (wt/wt, 1:1.2) was dissolved in CF with a concentration of 7.0 mg/mL with respect to PM6. DIO was then added to the solution at a volume fraction of 0% and 2%. The PM6:BTP-eC9 (wt/wt, 1:1.2) was dissolved in o-Xylene with a concentration of 10.0 mg/mL with respect to PM6. DIO was then added to the solution at a volume fraction of 0% and 0.5%. The D18:BTP-eC9 (wt/wt, 1:1.2) was dissolved in o-Xylene with a concentration of 6.5 mg/mL with respect to PM6. DIO was then added to the solution at a volume fraction of 0% and 0.5%. The PM6:L8-BO (wt/wt, 1:1.2) was dissolved in CF with a concentration of 8.0 mg/mL with respect to PM6. DIO was then added to the solution at a volume fraction of 0% and 0.5%.

The PM6 was dissolved in CB at a concentration of 10.0 mg/ml. DIO was then added to the PM6 solution at a volume fraction of 0% or 2%. The Y6 was dissolved in CF at a concentration of 10.0 mg/ml.

0.5% FS-30 was added to the original PEDOT:PSS solution for improving wetting on PM6 layer. All of the organic solutions were keep stirring for at least 3 hours before using.

Preparation of the PM6 film

First, the clean glass substrate was treated with ultraviolet ozone for 15 min. The PEDOT:PSS solution was spun onto the glass at 3000 rpm for 30 s. Then, the PM6 solution was spun onto the

top of the PEDOT:PSS layer at 5000 rpm for 30 s. Then, the glass/PEDOT:PSS/PM6 was placed in deionized water, and after about 5-10 s, the PM6 film automatically detached from the glass substrate and floated on the water surface.

Device fabrication

Organic solar cells (OSCs) with the ITO/ZnO/active layer/MoO_3 or PEDOT:PSS or PEDOT:F/Ag configuration were fabricated according to the following procedure. The ITO glass substrates were sequentially pre-cleaned in the ultrasonic baths containing detergent, deionized water, acetone, ethanol and isopropanol for 20 min, respectively. Then the cleaned ITO substrates were dried with nitrogen gas and then treated with ultraviolet-ozone for 15 min. The ZnO solution was spin-coated on ITO substrates at 4000 rounds per minute (rpm) for 30 s and then annealed at 150 °C for 30 min in air. Then the ITO substrates with ZnO films were transferred into a high-purity nitrogen-filled glove box. For the BHJ device, the PM6:Y6 and PM6:L8-BO blend solution was spin-coated onto the top of the ITO/ZnO at 3000 rpm for 40 s. PM6:BTP-eC9 and D18:BTP-eC9 was bladed coated in nitrogen with coating speed of 10 mm/s. For the PHJ device, the Y6 solution was spin-coated onto ITO/ZnO at 3000 rpm for 40 s, then the PM6 film floating on the water surface was transferred to ITO/ZnO/Y6. Last, the active layers of the prepared BHJ and PHJ structures were annealed at 100 °C for 10 min. A thin MoO_3 layer (10 nm) and a silver (Ag) layer (100 nm) were sequentially deposited by thermal evaporation under 2.5×10^{-4} Pa and the thickness was monitored by a quartz crystal microbalance. For devices with PEDOT:PSS as hole transport layer (HTL), PEDOT:PSS with 0.5% FS-30 was spin-coated on top of PM6 at a speed of 4000 rpm. PEDOT:F was spin-coated on top of PM6 at a speed of 4000 rpm. Then 100 nm Ag was evaporated as electrode. The active area of each device is approximately 0.063 cm^2, which is defined by the vertical overlap of the ITO cathode and Ag anode.

Device characterization

The current density-voltage (J-V) curves of the OSCs were measured under 1 sun AM 1.5 G illumination (100 mW/cm^2) using a Keithley 2400 source meter in a high-purity nitrogen-filled glove box. The AM 1.5 G illumination was simulated using a solar simulator and calibrated by a

standard silicon cell. The external quantum efficiency (EQE) data were collected by using a commercial 7-SCSpec system under air conditions.

Surface morphology characterization

The grazing-incidence wide-angle X-ray scattering (GIWAXS) and grazing-incidence small-angle X-ray scattering (GISAXS) measurements of active layers were performed at Xenocs in-house X-ray scattering beamline (Xeuss 3.0). X-ray had a wavelength of 1.5419 Å and the sample-to-detector distance was calibrated using a silver behenate standard. The samples for GIWAXS and GISAXS measurements were deposited onto silicon substrates.

The scattering intensity is modeled as

$$I(q) = A1 < P(q,R,z) > S(q,R) + A2DAB(q) + A3 \quad \text{(Equation S1)}$$

Here, A1, A2, A3 are prefactors, the background signal is modeled as DAB(q) with DAB model:[1]

$$DAB(q) = \frac{8\pi\xi_{DAB}^{3}}{(1+q^{2}\xi_{DAB}^{2})^{2}} \quad \text{(Equation S2)}$$

where ξ_{DAB} is the correlation length of amorphous intermixing phases. < P(q, R, z) > is the averaged form factor. Here, we employ the spherical form factor P(q, r) following Schulz distribution f(r, R, z) with the mean radius R and radius distribution z > -1:[2]

$$P(q,r) = \left[\frac{3(\sin qr - qr\cos qr)}{(qr)^{3}}\right]^{2} \quad \text{(Equation S3)}$$

$$f(r,R,z) = \left(\frac{z+1}{R}\right)^{z+1} r^{z} exp\left[-\left(\frac{z+1}{R}r\right)\right]\frac{1}{\Gamma(z+1)} \quad \text{(Equation S4)}$$

$$< P(q,R,z) >= \int_{0}^{\infty} P(q,r)f(r,R,z)dr \quad \text{(Equation S5)}$$

where $\Gamma(z+1)$ is the Gamma function. S(q, R) is the structure factor which may differ for different systems.

For the D18: L8-BO system, we mainly used a fractal-like network structure factor:[3]

$$S_{f}(q,R,\eta) = 1 + \frac{\sin\left[(D-1)\tan^{-1}(q\eta)\right]}{(qR)^{D}} \frac{D\Gamma(D-1)}{\left[1+1/(q\eta^{2})\right]^{(D-1)/2}} \quad \text{(Equation S6)}$$

where η is the correlation length of the fractal-like network formed by the aggregation of primary

particles with the mean radius R. Here, the primary particles correspond to small molecular crystallites and the correlation length corresponds to the pure phase domain. The fractal dimension D is fixed to 3 here. The domain size of pure phase is determined by $2R_g$, where $Rg = [D(1+D)/2]^{1/2}\eta$ is the gyration radius of this fractal-like network.

Photo-induced force microscopy (PiFM)

The PIFM instrument model is NanoIR2-fs, with a spatial resolution of 10 nm. The sample substrate is a 1.5 × 1.5 cm white glass plate, which is then mounted onto a magnetic iron plate.

Kelvin probe force microscopy (KPFM)

Measurements were performed with Bruker Dimension icon mode AFM, equipped with a Bruker SCM-PIT conductive probe (Pt/Ir. resonance frequency 60-90 kHZ, k=1.2-5.5 N/m, R_C = 25 nm). All KPFM scans were performed in an open system, utilizing the lift mode. The lift height was set to 10 nm and a direct current (DC) bias voltage of 2000 mV was applied.

Photocurrent density (J_{ph}) versus effective voltage (V_{eff}) measurements

The J_{ph} versus V_{eff} curves, $J_{ph} = J_{light} - J_{dark}$, where J_{light} and J_{dark} are the current densities under illumination and in dark, respectively. And $V_{eff} = V_0 - V_{bias}$, where V_0 is the voltage at which J_{ph} is equal to 0 and V_{bias} is the applied bias voltage. The charge collection probability (P_{coll}) are calculated by $P_{coll} = J_{ph}/J_{sat}$, ($J_{sat}$, current densities at saturation condition) under the maximum power output conditions.

Light intensity dependence measurements for V_{OC}

The relationship of V_{OC} dependence on P_{light} indicates the degree of trap-assisted recombination, which have the relation of $V_{OC} \propto n(kT/q)ln(P_{light})$, where k is the Boltzmann constant, T is the absolute temperature, q is the elementary charge, and n is the ideality factor under illumination and presents the recombination dynamics in the device. The slope of the $V_{OC} - P_{light}$ curve could be higher than kT/q when the trap-assisted recombination is involved.

Calculation of open-circuit voltage loss

We divided the open circuit voltage losses (ΔV) into two parts, one for non-radiative losses (ΔV_{nr}) and the rest of the losses were classified as other forms of voltage losses (ΔV_{other}), where ΔV is equal to $E_g - V_{OC}$, ΔV_{nr} is equal to the differences between radiative recombination limit $V_{OC,rad}$ (calculated according to Equation S9) and V_{OC}, and ΔV_{other} is equal to $\Delta V - \Delta V_{nr}$.

E_g is the band gap energy of the solar cells, which was calculated from Sensitive-EQE according to Equation S7:[4]

$$E_g = \frac{\int_a^b E * P(E)dE}{\int_a^b P(E)dE} \quad \text{(Equation S7)}$$

where the $P(E)$ is the distribution of band-gap energies and equal to $dEQE/dE$. The integration limits a and b are chosen as the energy where $P(E)$ is equal to 50% of its maximum.

$$V_{OC,rad} = \frac{kT}{q}\ln\left(\frac{J_{SC}}{J_0^{rad}} + 1\right) \cong \frac{kT}{q}\ln\left(\frac{q\int_0^{+\infty} EQE(E)\emptyset_{AM_{1.5}}(E)dE}{q\int_a^{+\infty} EQE(E)\emptyset_{BB}(E)dE}\right) \quad \text{(Equation S8)}$$

Here, k is Boltzmann's constant, T is the temperature of the solar cell (T = 300 K is used in this paper), q is elementary charge, and $\phi_{BB}(E)$ is the black body spectrum at the temperature T of the solar cell.[5]

Device stability characterization

The stability test results of the device were obtained by MPP degradation setup equipment (Automatic Research GmbH, Germany).[6] Devices were sealed in glass-fronted chambers under N_2 without moisture. An array of white LEDs was used as light source with intensity equivalent to 1

sun. The temperature of the cells was kept 28-32 ℃ by a fan and water-cooling device during measurements. For maintain a nitrogen atmosphere, the pure nitrogen gas was continuously fluxing into the chamber during measurements.

X-ray photoelectron spectroscopy (XPS)

XPS testing was performed on the sample/Si substrate using ESCALAB XI+ instrument (Thermo Fisher, America). Source gun type is Al K Alpha. Spot size is 500 μm. Energy step size is 0.050 eV. Number of energy steps is 400-600.

UV-vis absorption spectra

The UV-vis absorption spectra were recorded by spectral analyzer (Shenzhen Longmeida Technology Co., Ltd., APL-AS-96). Each film test has six fixed positions, designated as (1,1), (1,2), (1,3), (2,1), (2,2), and (2,3).

Electron Paramagnetic Resonance (EPR)

X-band (9.2-9.9 GHz) EPR measurements were performed with CIQTEK EPR200-Plus. The films were deposited on ultra-thin glass, cut to 3 mm wide and 20 mm long pieces and then inserted into a quartz EPR tube. The samples were sealed in nitrogen atmosphere in the quartz tube to avoid exposure to air throughout the measurement.

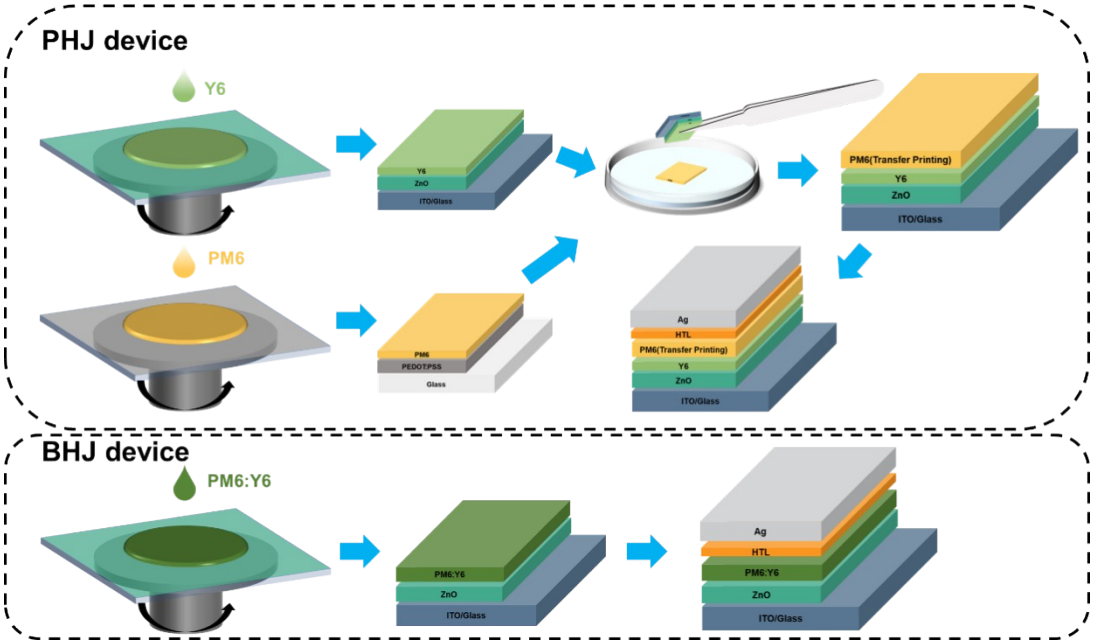

Fig. S1. Schematic of the PHJ and BHJ device fabrication process.

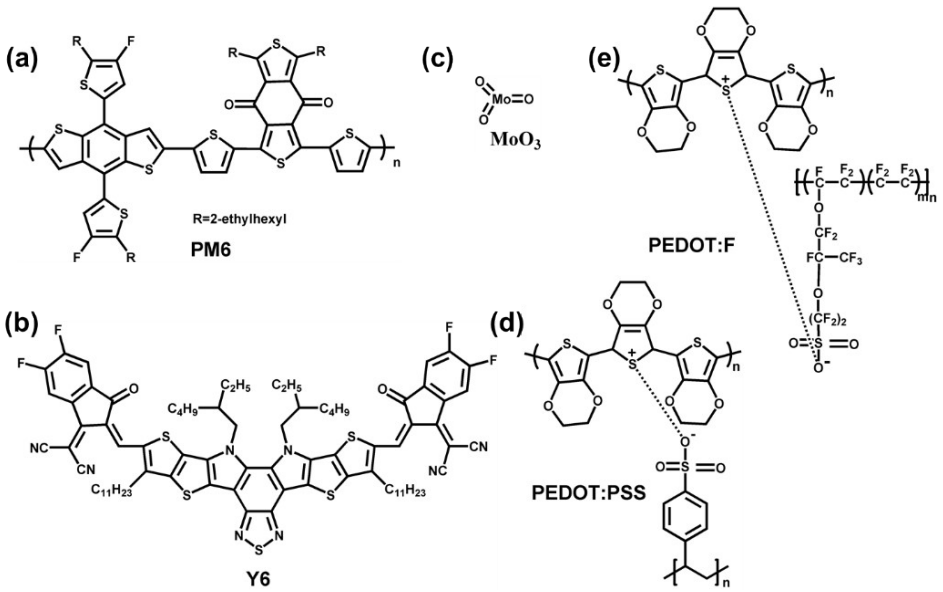

Fig. S2. Chemical structures of a) PM6, b) Y6, c) MoO_3, d) PEDOT:PSS and e) PEDOT:F.

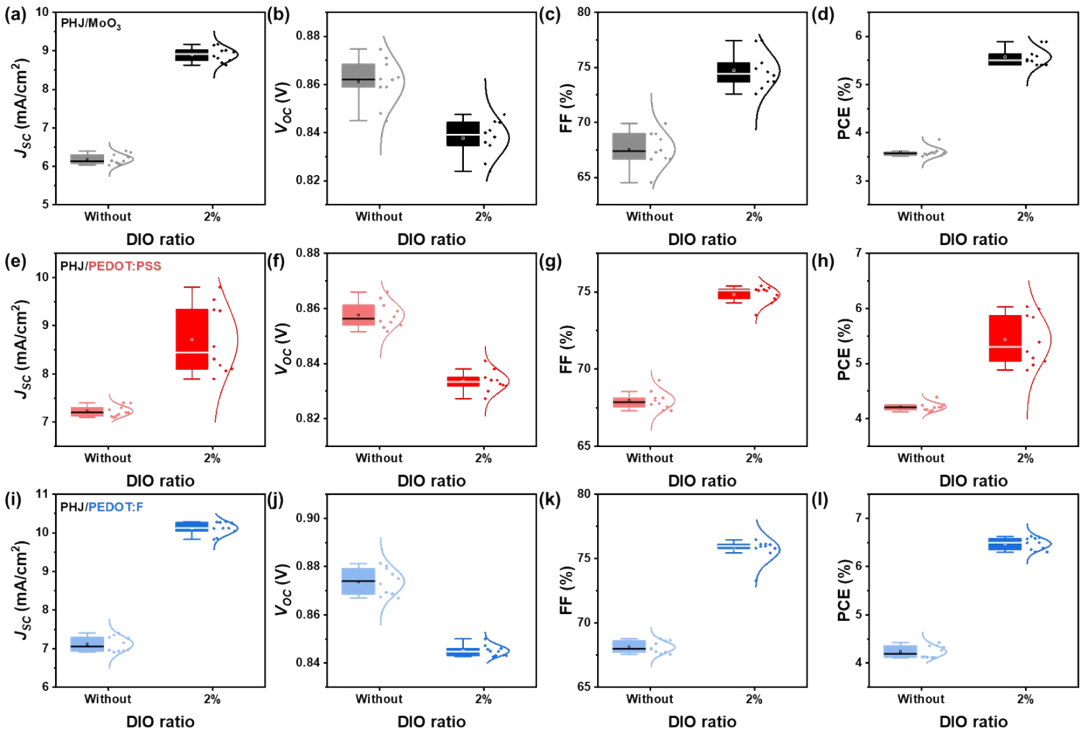

Fig. S3. Box plot of photovoltaic parameters for PHJ devices with a-d) MoO_3, e-h) PEDOT:PSS and i-l) PEDOT:F as HTL.

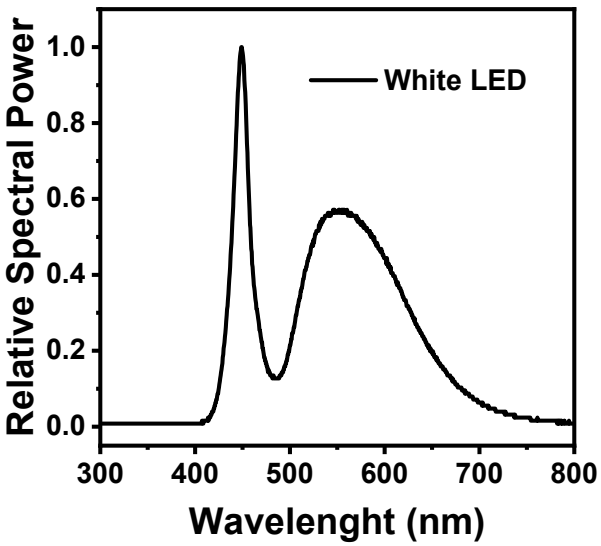

Fig. S4. Light spectrum of the LEDs used for stability test in this work was obtained from the laboratory test.

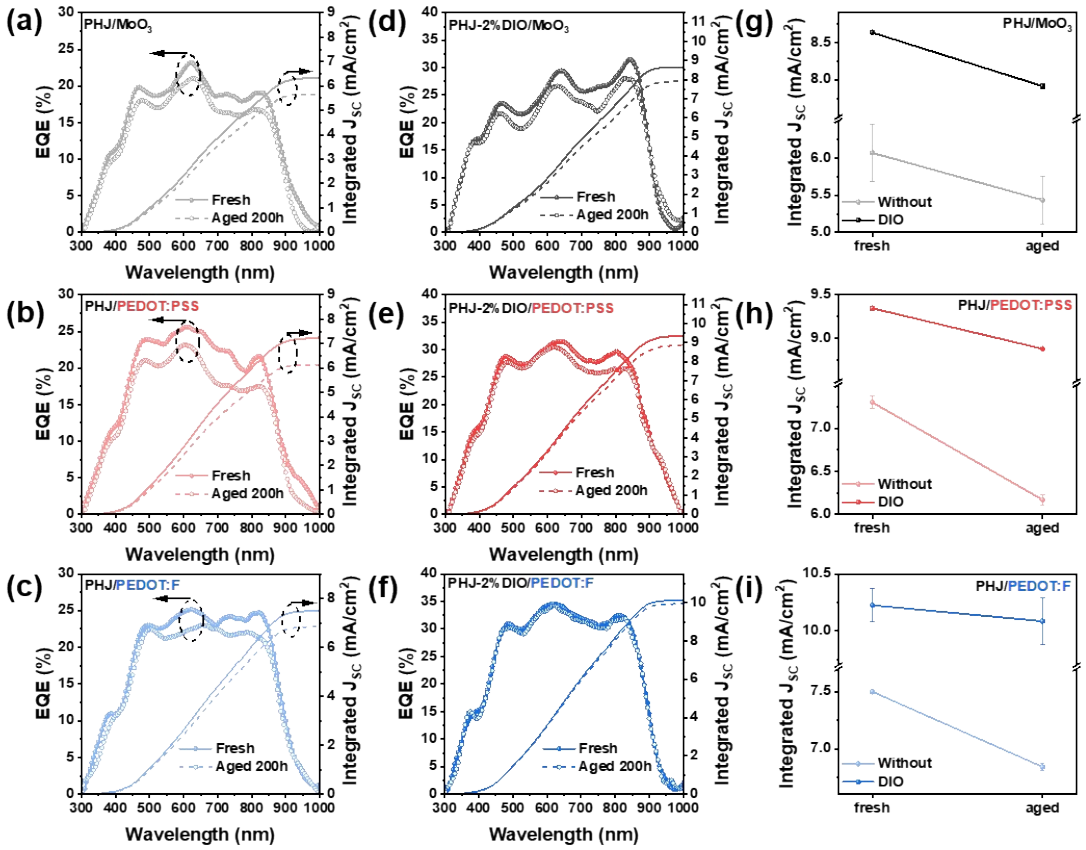

Fig. S5. a-f) The EQE spectra evolution and integrated J_{SC} of the PHJ device with different HTL before and after photo aging. g-i) Integrated J_{SC} of different PHJ devices before and after photo aging averaged from 2 devices.

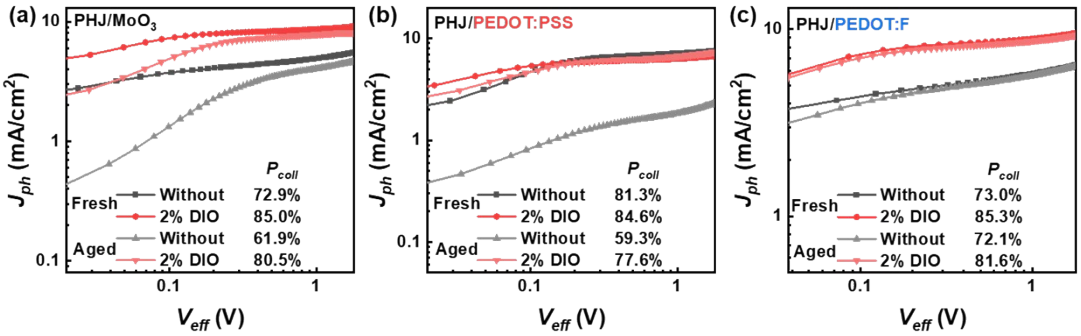

Fig. S6. The effective voltage (V_{eff}) versus photocurrent density (J_{ph}) evolution of the PHJ device with a) MoO_3, b) PEDOT:PSS and c) PEDOT:F before and after photo aging.

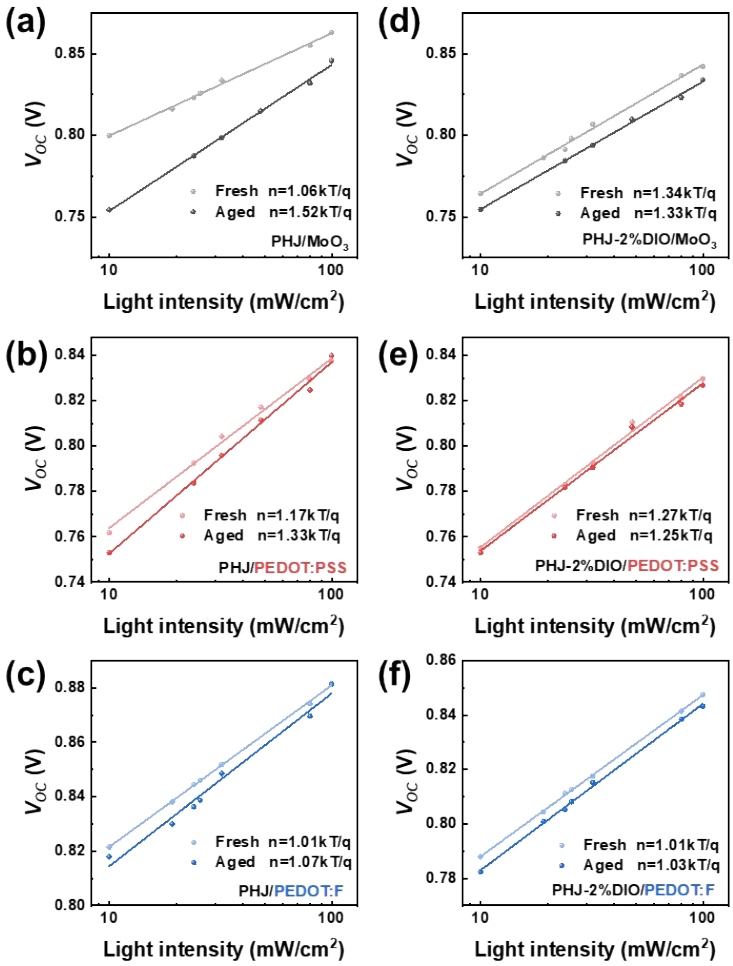

Fig. S7. Measurement of the light intensity dependence of V_{OC} in PHJ devices a-c) without and d-f) with DIO before and after photo aging.

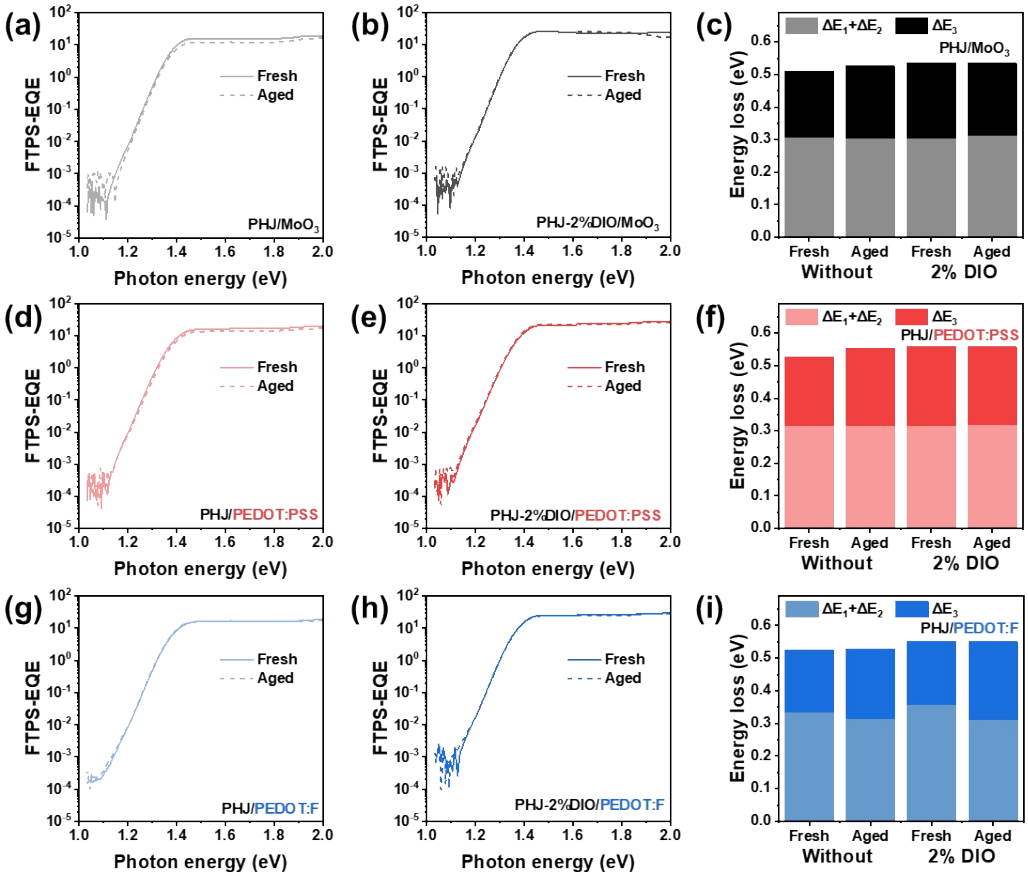

Fig. S8. FTPS-EQE and detailed energy losses of PHJ devices with a-c) MoO_3, d-f) PEDOT:PSS and g-i) PEDOT:F before and after photo aging.

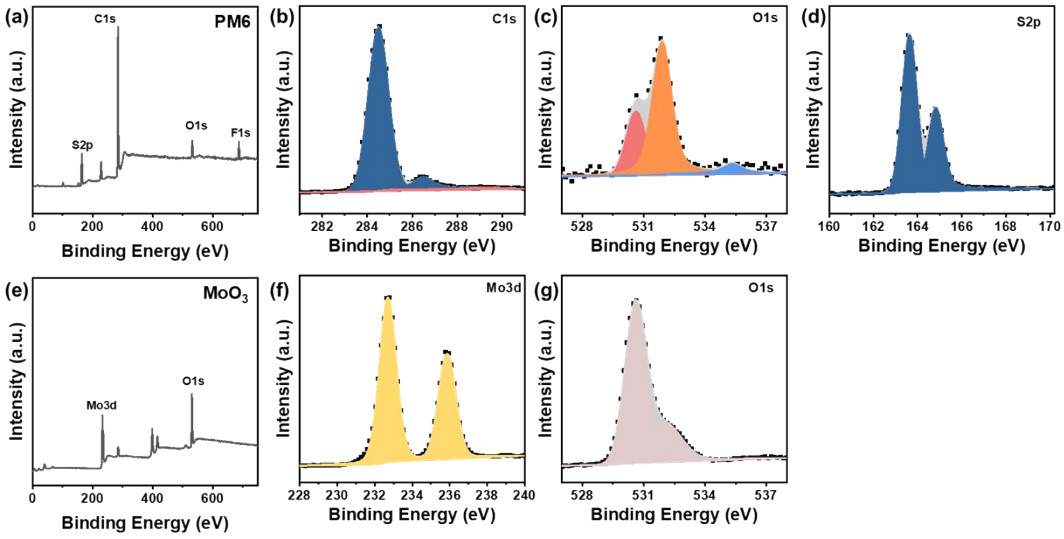

Fig. S9. XPS measurement of a-d) PM6 and e-g) MoO_3 films.

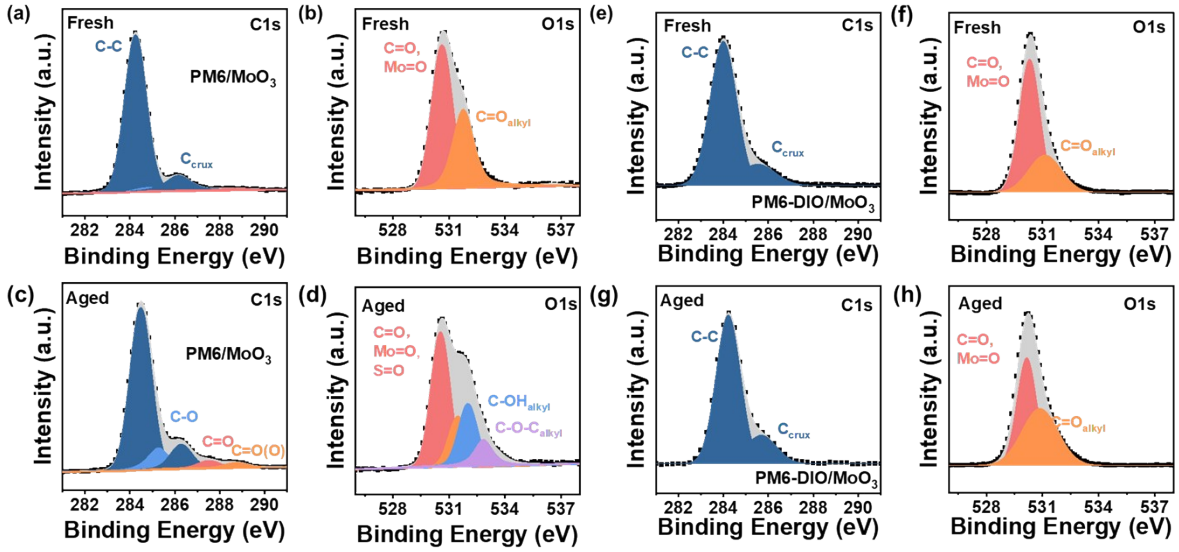

Fig. S10. XPS measurements of a-d) $PM6/MoO_3$ and e-h) $PM6\text{-}DIO/MoO_3$ films before and after photo aging.

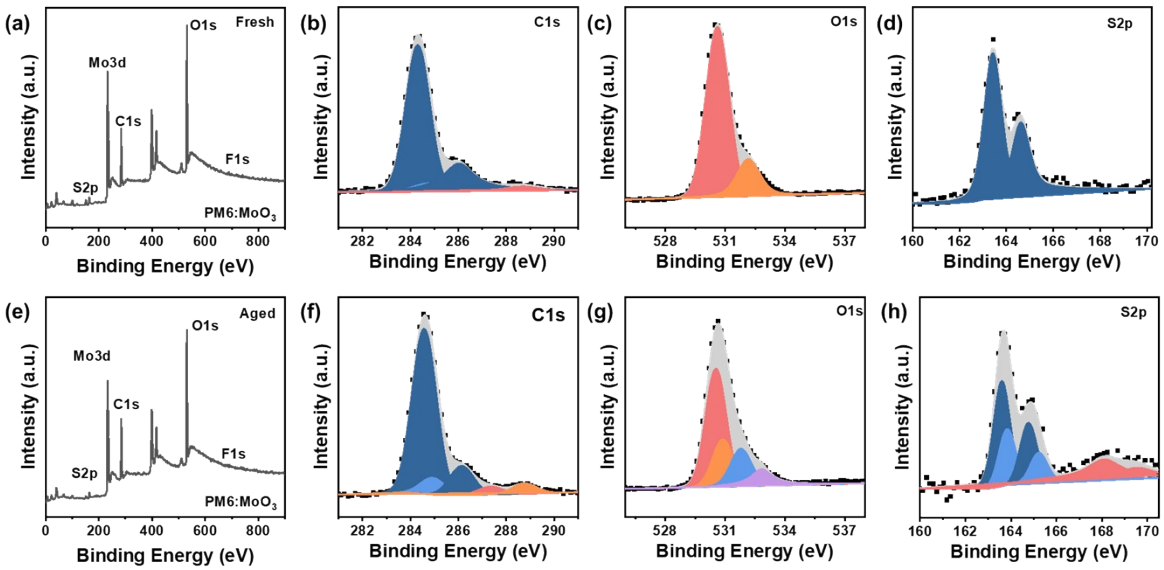

Fig. S11. XPS measurements of PM6:MoO_3 blend film a-d) before and e-h) after photo aging.

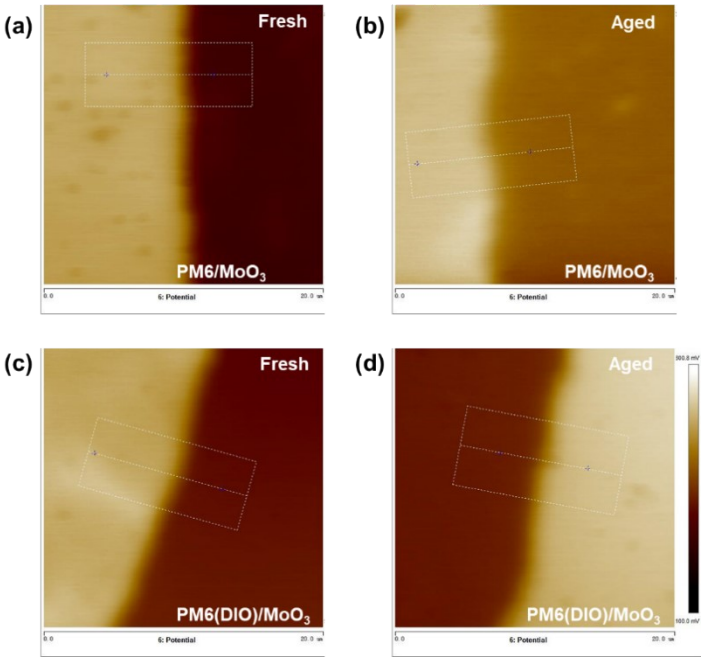

Fig. S12. CPD images of a-b) $PM6/MoO_3$ and c-d) $PM6\text{-}DIO/MoO_3$ film before and after photo aging. Take the CPD values of the three long sides of the dashed white box in the image, then calculate their average.

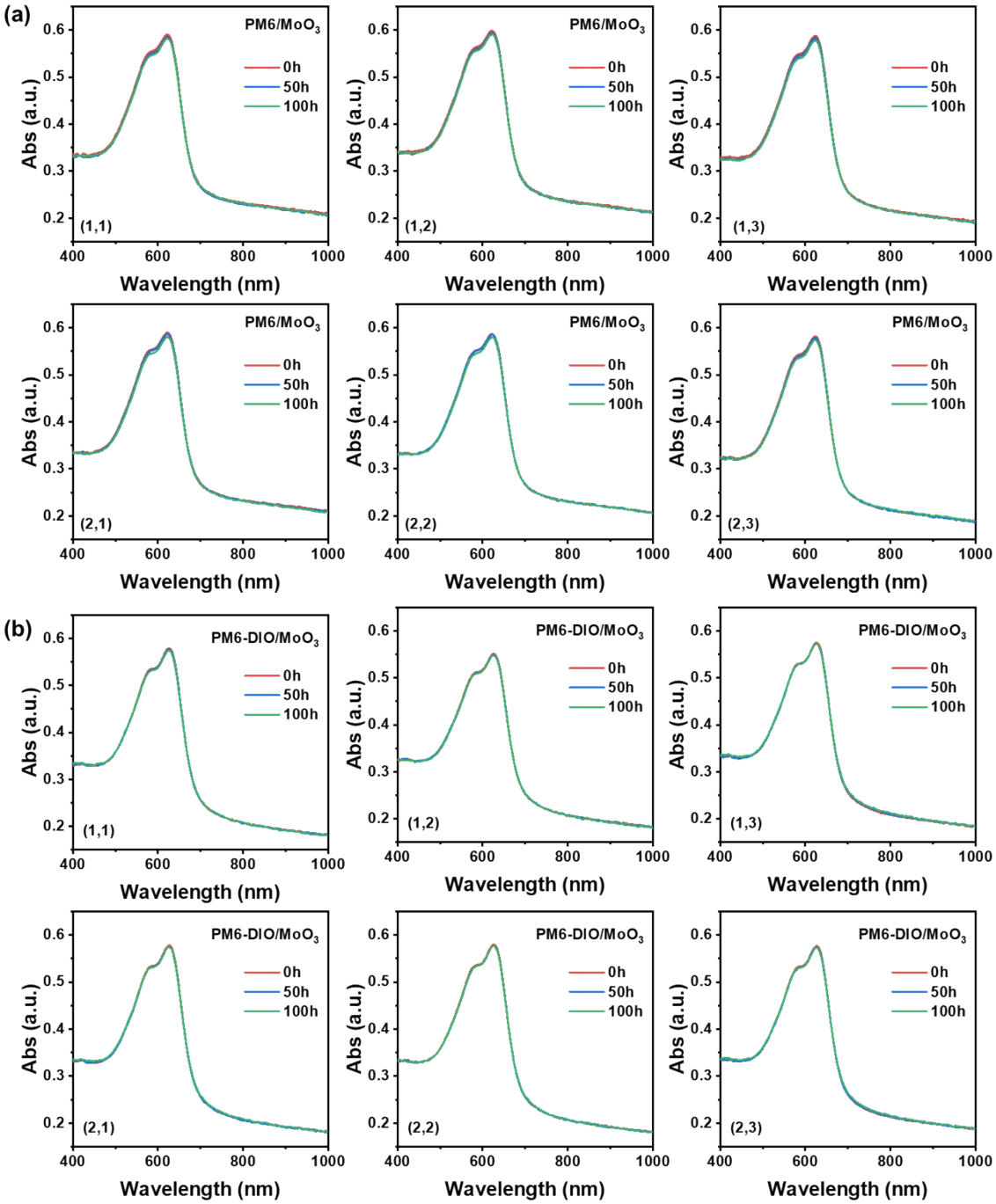

Fig. S13 Absorption spectrum evolution of encapsulated PM6/MoO_3 films during photoaging process.

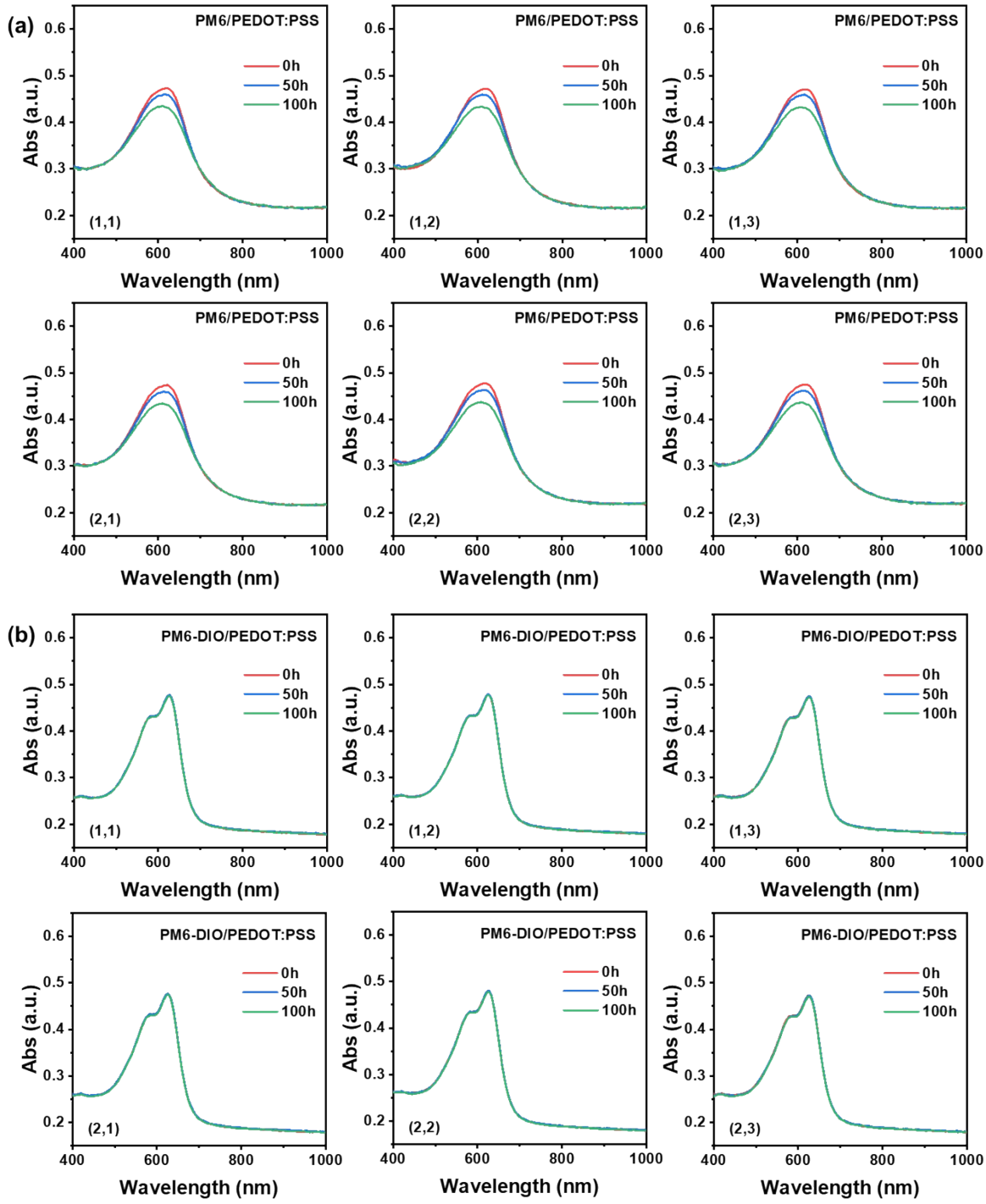

Fig. S14 Absorption spectrum evolution of encapsulated PM6/PEDOT:PSS films during photoaging process.

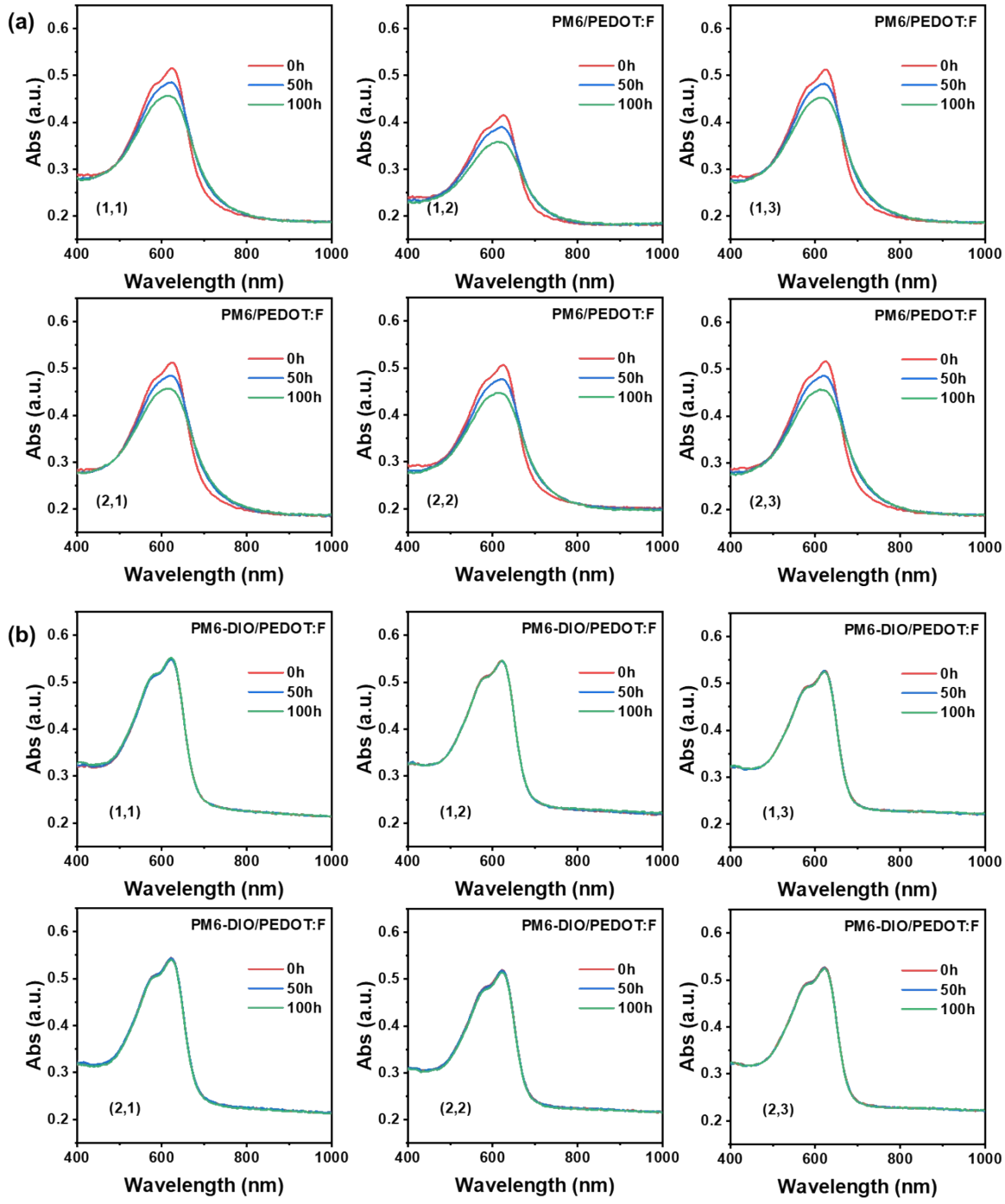

Fig. S15 Absorption spectrum evolution of encapsulated PM6/PEDOT:F films during photoaging process.

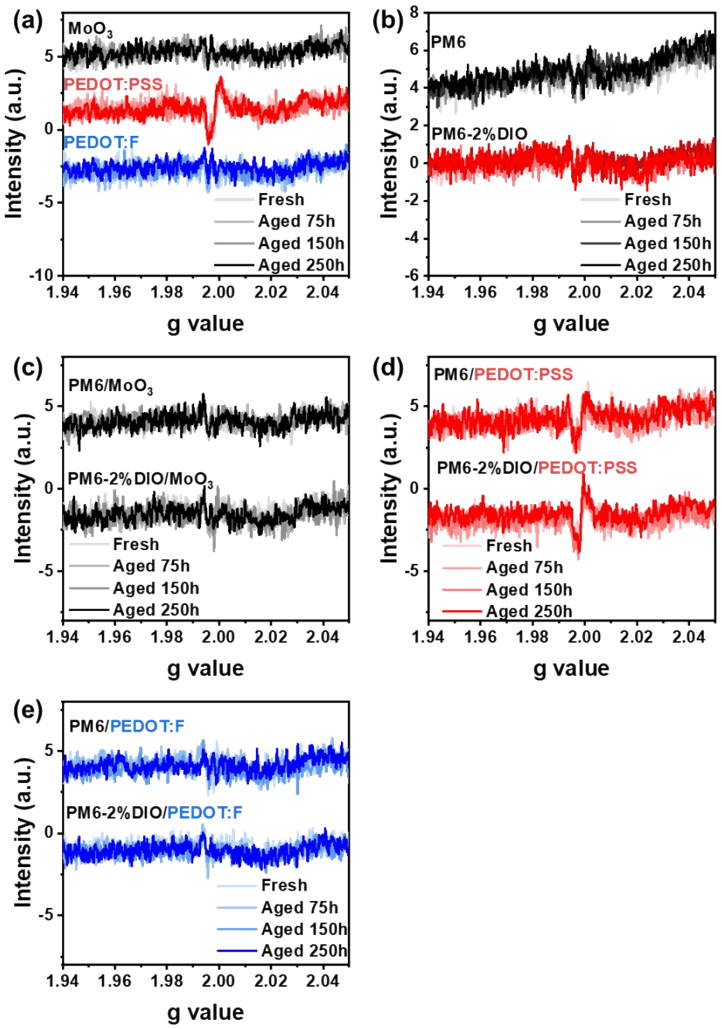

Fig. S16. Evolution of EPR spectra for a) HTL, b) PM6, c) PM6/MoO_3, d) PM6/PEDOT:PSS and e) PM6/PEDOT:F films before and after photo aging.

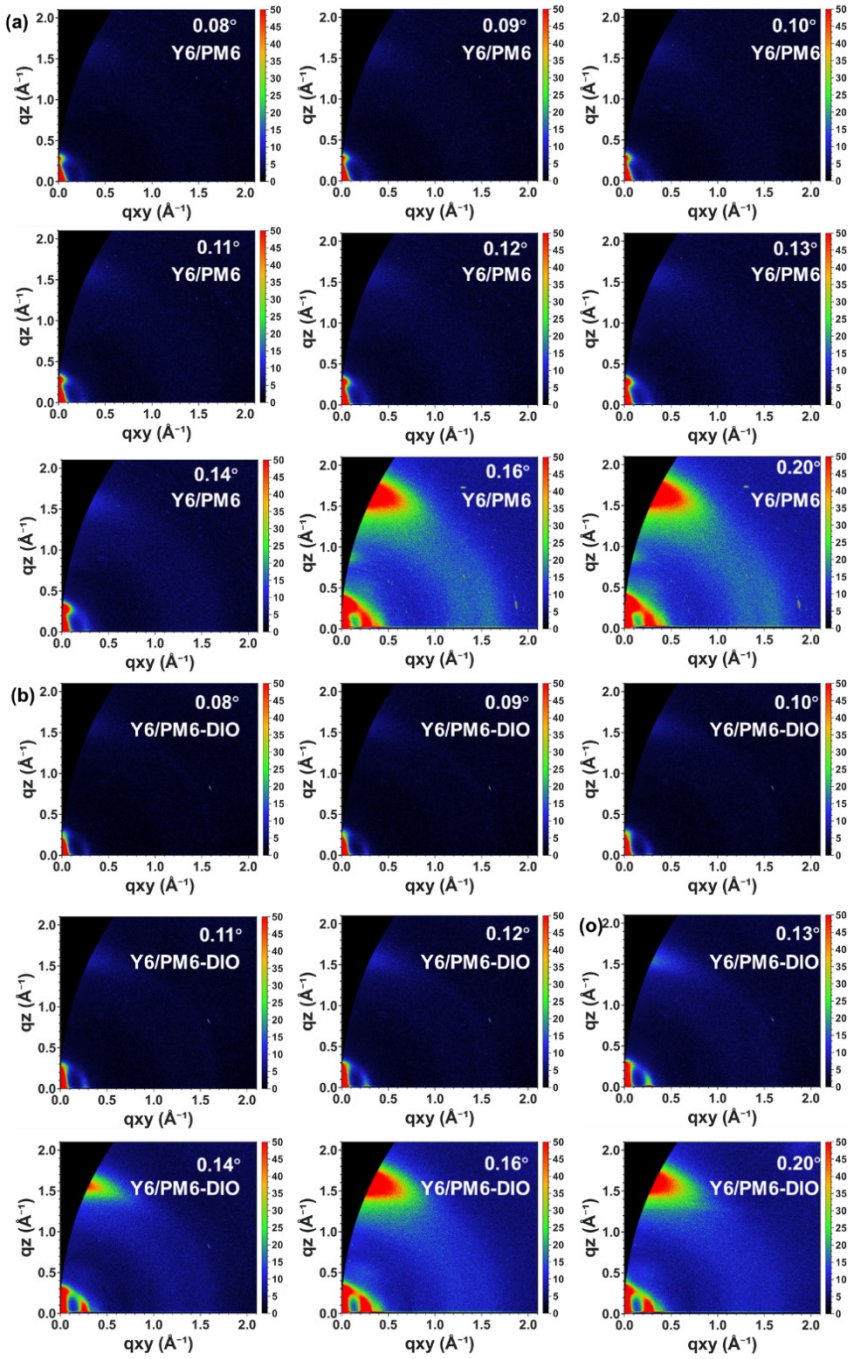

Fig. S17. 2D GIWAXS patterns obtained from Y6/PM6 films a-i) without and j-r) with DIO at different incident angles.

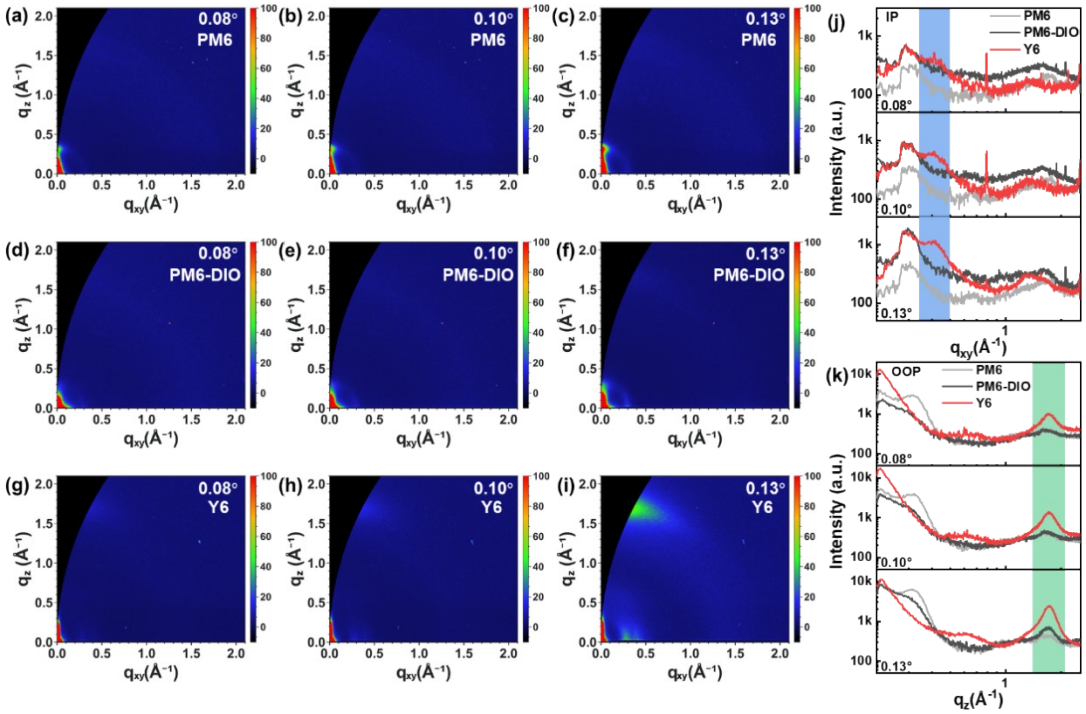

Fig. S18. a-i) 2D GIWAXS images and j-k) 1D GIWAXS profiles of PM6 and Y6 films at different incident angles.

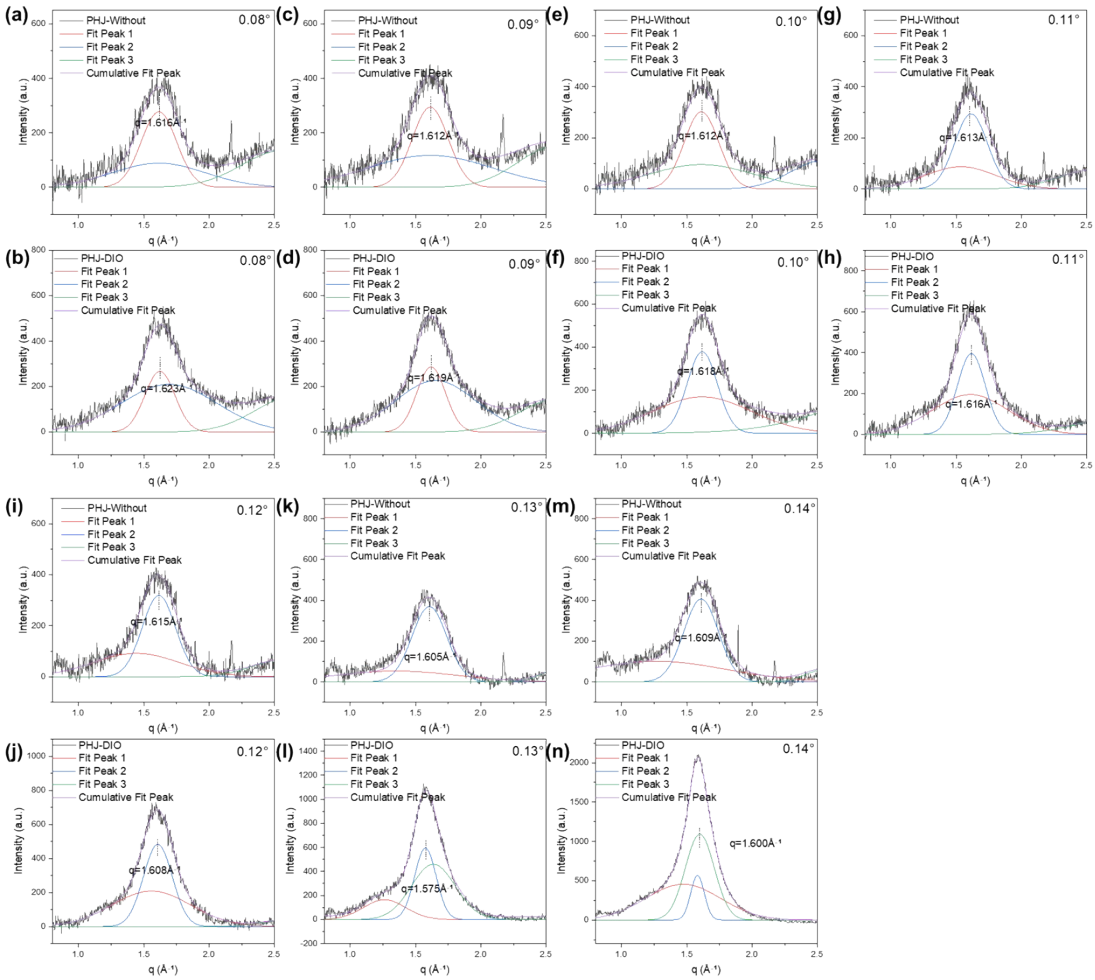

Fig. S19. a-n) GIWAXS fitting result of PHJ film at different incident angles along OOP direction.

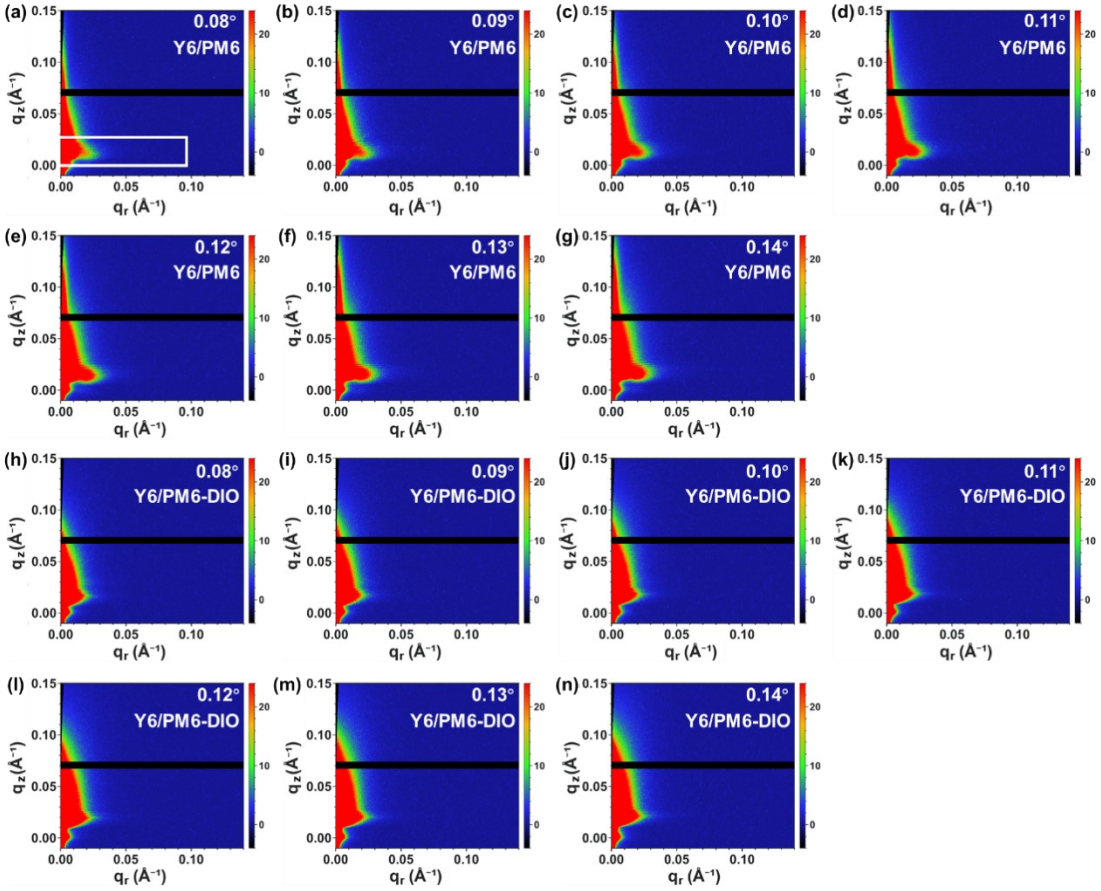

Fig. S20. 2D GISAXS patterns obtained from Y6/PM6 films a-g) without and h-n) with DIO at different incident angles (extract 1D profiles from the highlighted integration area in the white rectangle).

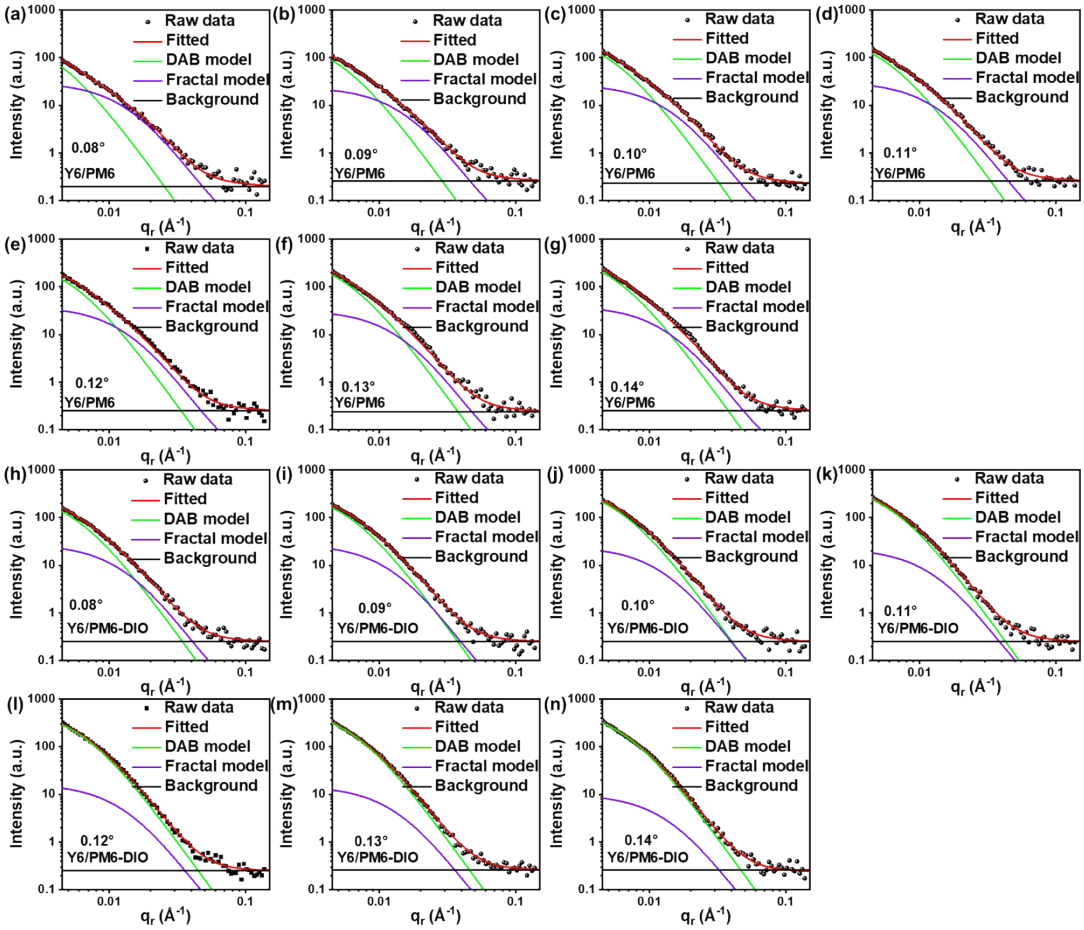

Fig. S21. GISAXS fitting result of PHJ film a-g) without and h-n) with DIO at different incident angles along IP direction.

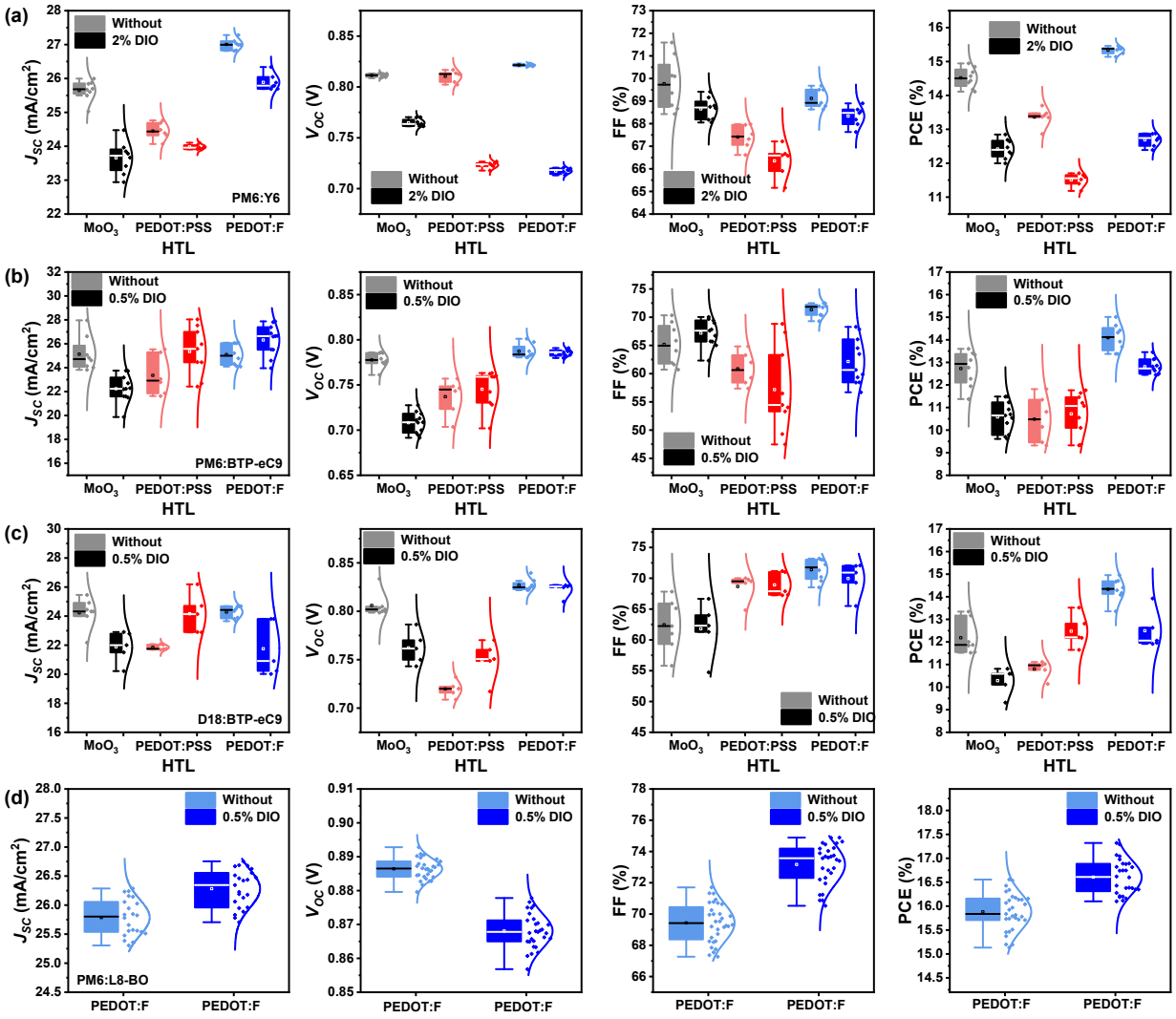

Fig. S22. Box plot of photovoltaic parameters for a) PM6:Y6, b) PM6:BTP-eC9, c) D18:BTP-eC9 and d) PM6:L8-BO devices with different HTLs.

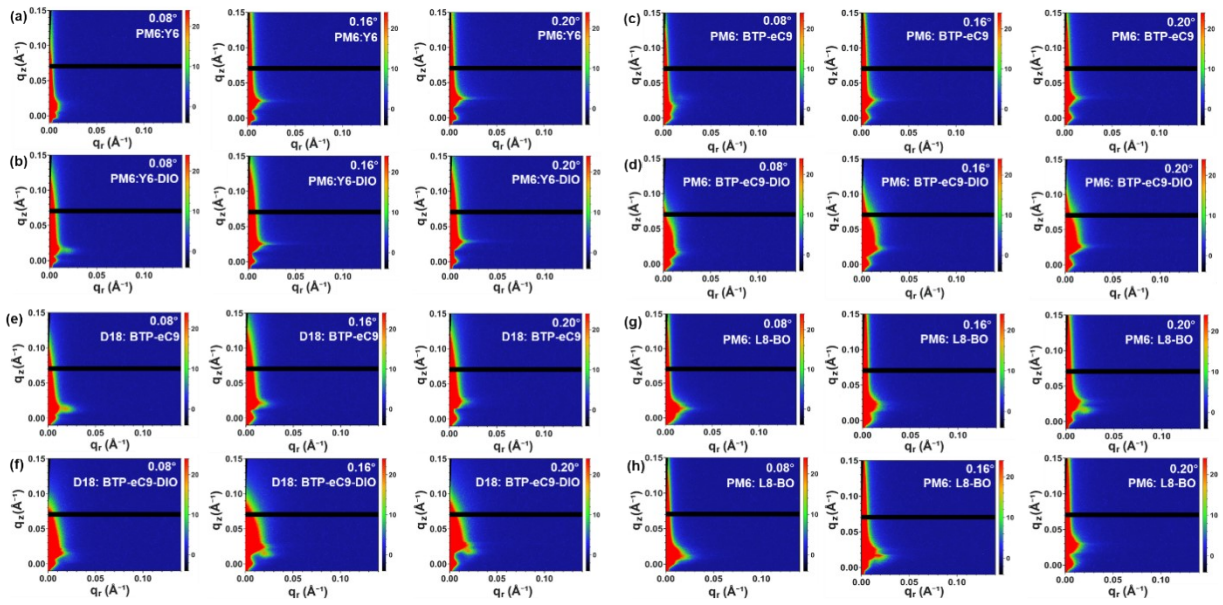

Fig. S23. 2D GISAXS patterns obtained from a-b) PM6:Y6, c-d) PM6:BTP-eC9, e-f) D18:BTP-eC9 and g-h) PM6:L8-BO films at different incident angles.

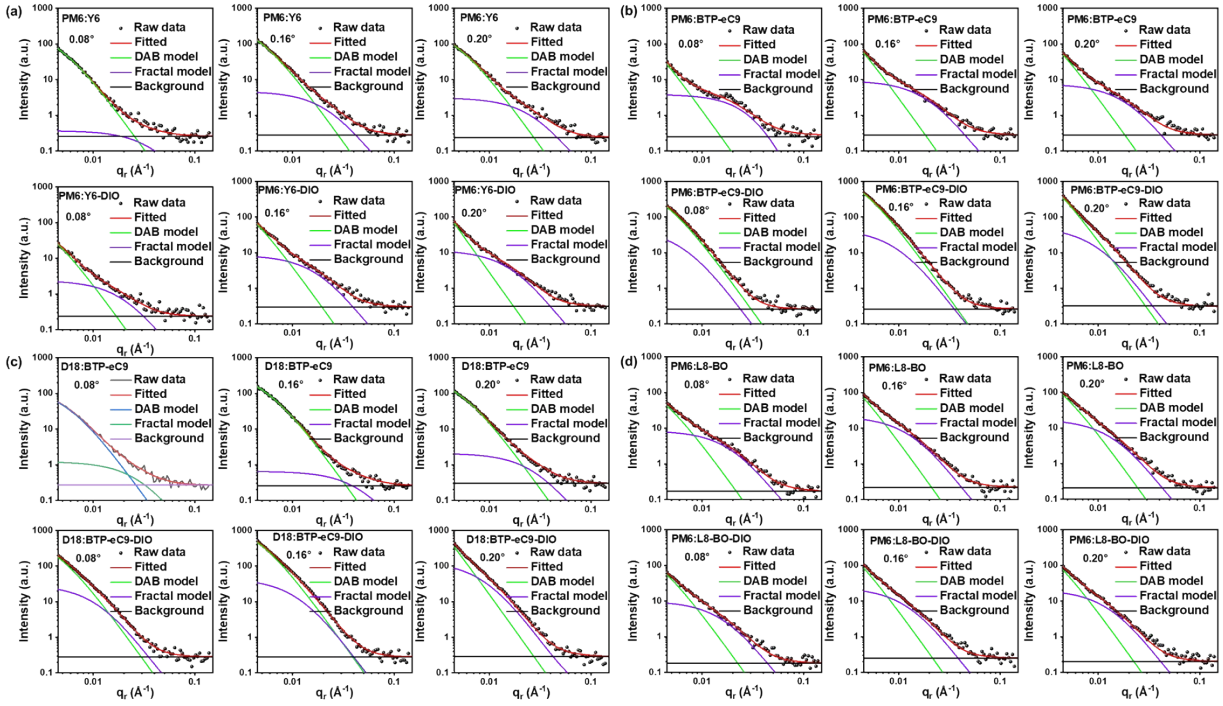

Fig. S24. GISAXS fitting result of a) PM6:Y6, b) PM6:BTP-eC9, c) D18:BTP-eC9 and d) PM6:L8-BO film at different incident angles along IP direction.

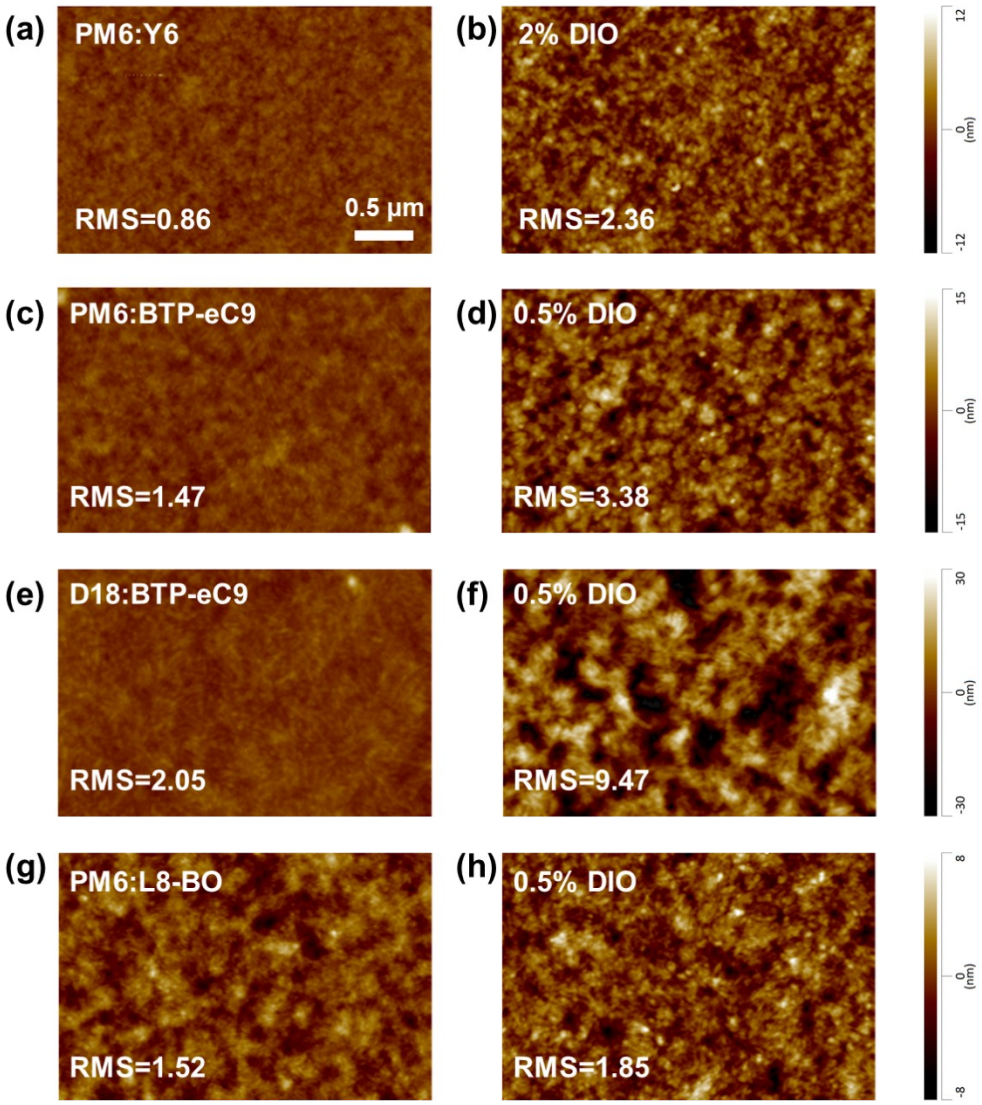

Fig. S25. AFM height images of a-b) PM6:Y6, c-d) PM6:BTP-eC9, e-f) D18:BTP-eC9 and g-h) PM6:L8-BO films

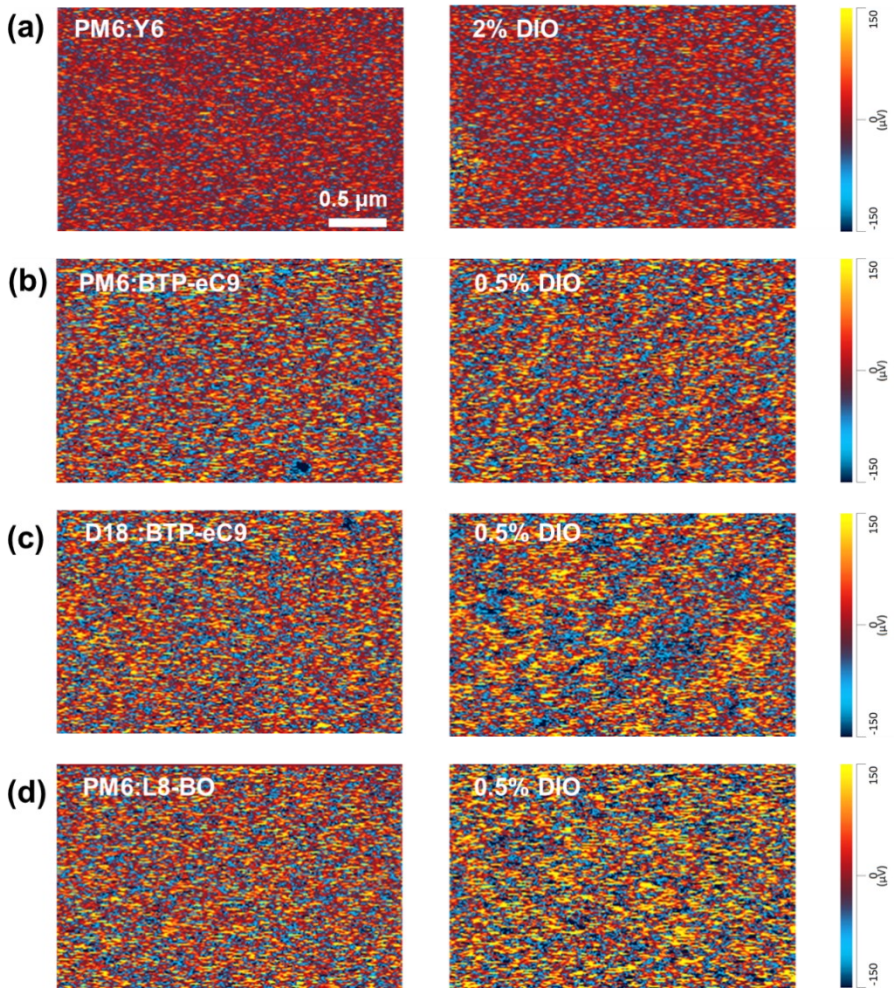

Fig. S26. AFM-IR composite images of BHJ films indicating acceptor-rich (high potential) regions based on IR absorption at the donor characteristic peak. a) PM6:Y6, Y6:1532 cm^{-1}, b) PM6:BTP-eC9, BTP-eC9:1530 cm^{-1}, c) D18:BTP-eC9, BTP-eC9:1530 cm^{-1} and d) PM6:L8-BO, L8-BO:1530 cm^{-1}.

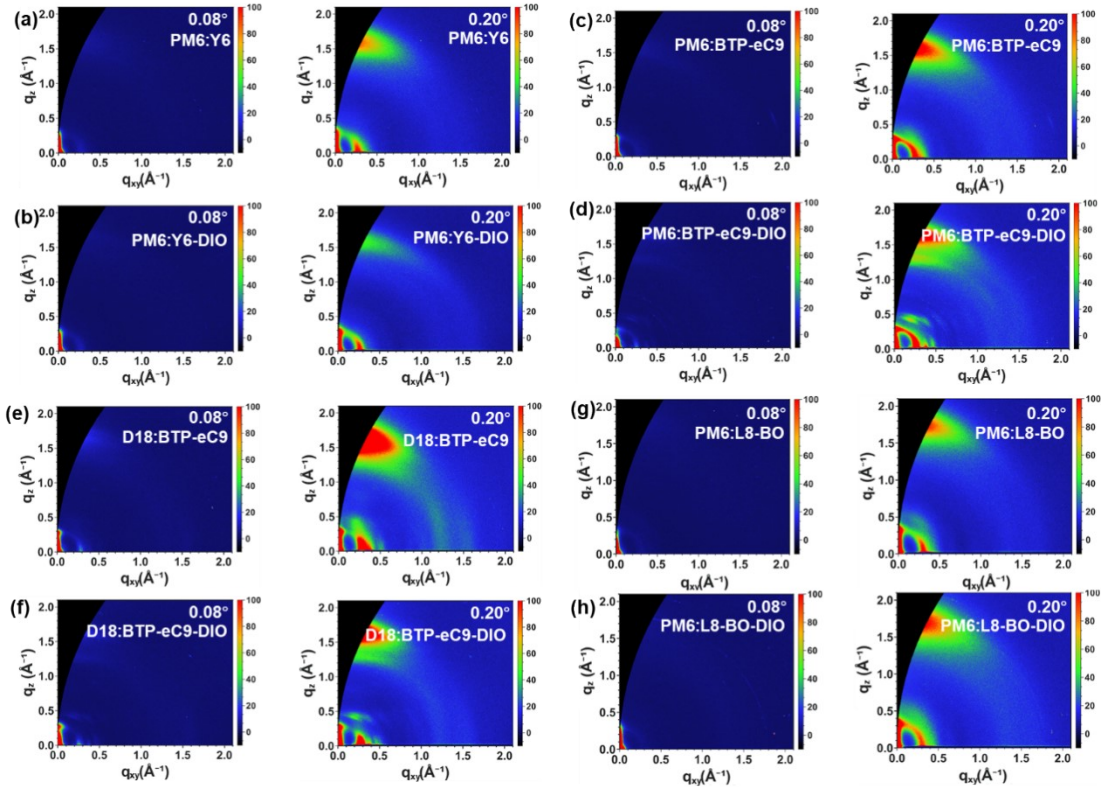

Fig. S27. 2D GIWAXS patterns obtained from a-b) PM6:Y6, c-d) PM6:BTP-eC9, e-f) D18:BTP-eC9 and g-h) PM6:L8-BO films at different incident angles (0.08° and 0.20°).

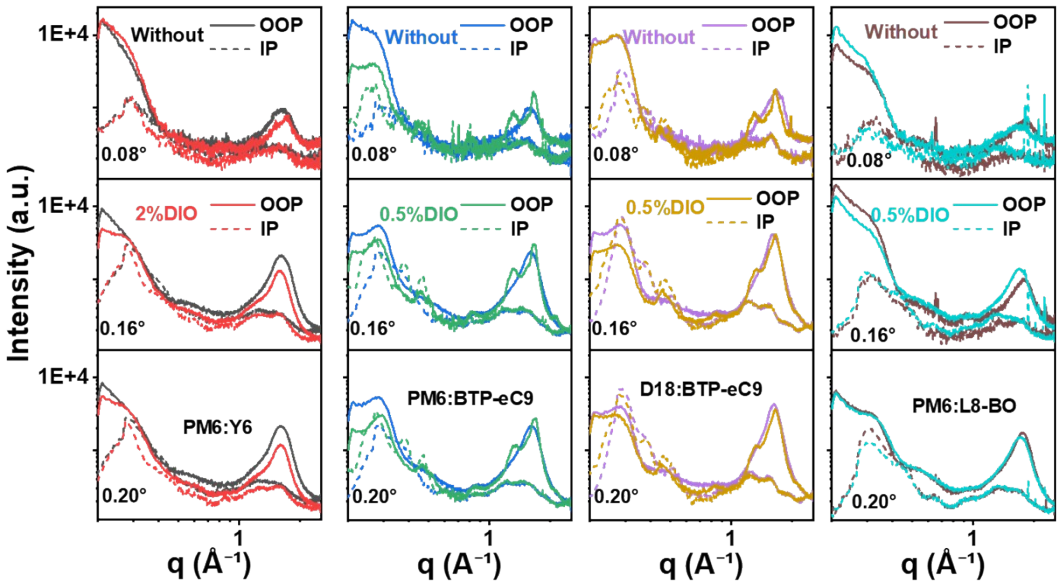

Fig. S28. 1D GIWAXS profiles of different BHJ films at different incident angles.

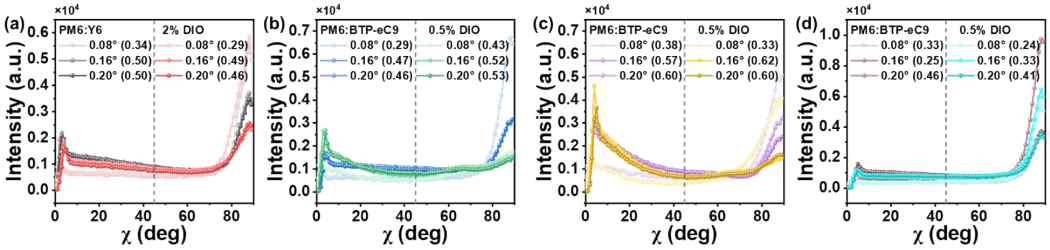

Fig. S29. Pole figures extracted from the lamellar diffraction (100) for the a) PM6:Y6, b) PM6:BTP-eC9, c) D18:BTP-eC9 and d) PM6:L8-BO films at different angles.

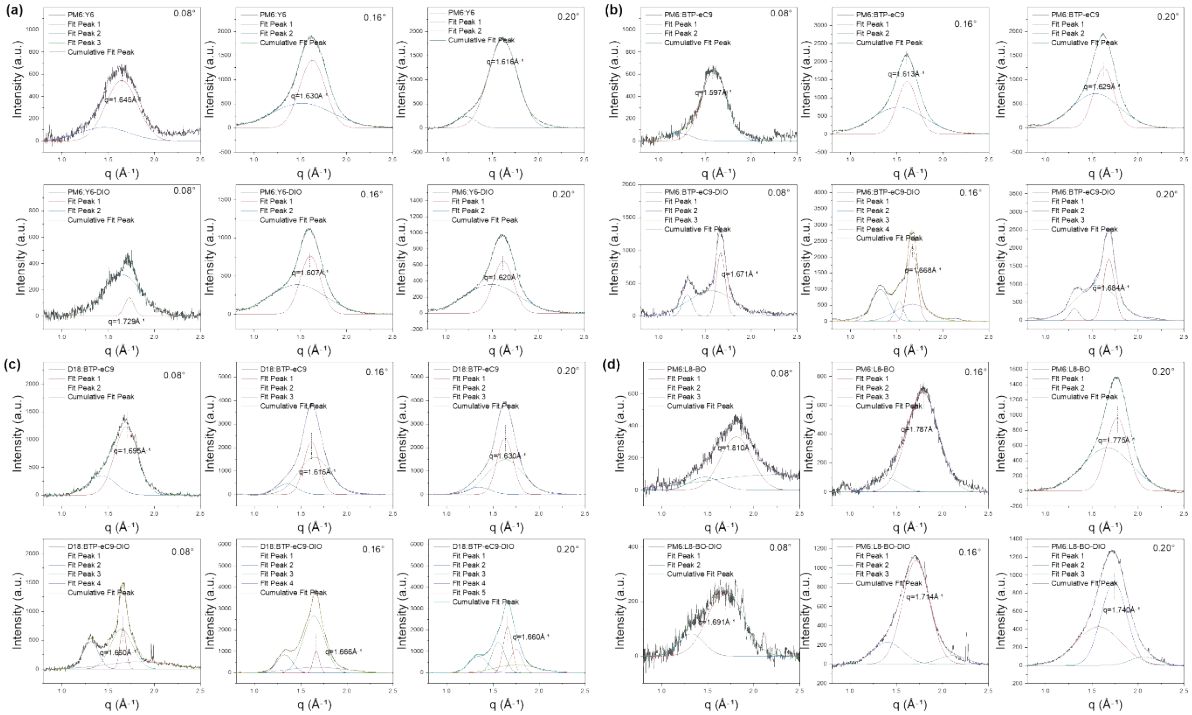

Fig. S30. GIWAXS fitting result of a) PM6:Y6, b) PM6:BTP-eC9, c) D18:BTP-eC9 and d) PM6:L8-BO at different incident angles along OOP direction

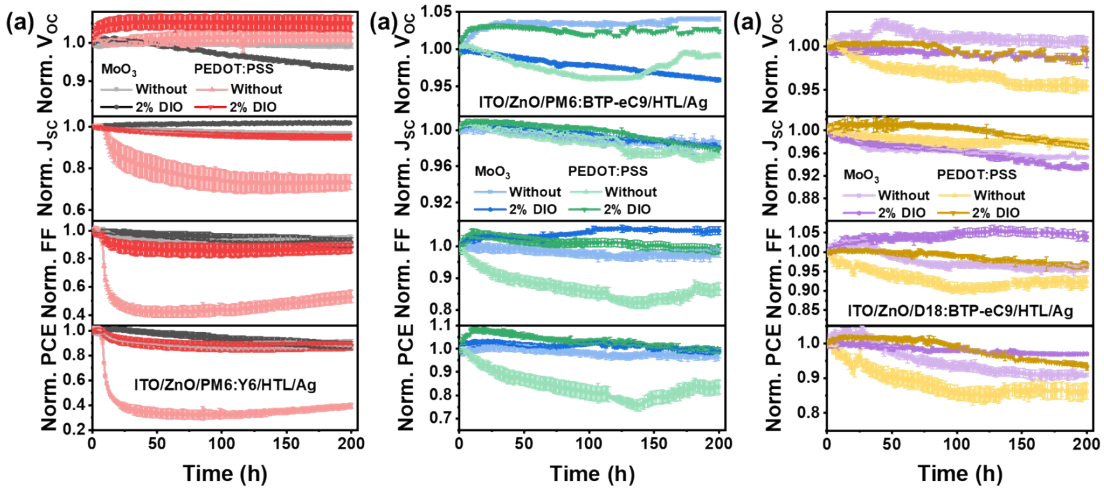

Fig. S31. The normalized photovoltaic parameters of a) PM6:Y6, b) PM6:BTP-eC9, and c) D18:BTP-eC9 devices under white LED illumination (1 sun intensity). During the stability measurement, the devices were kept in a nitrogen atmosphere. Normalized photovoltaic parameters are obtained by statistical analysis of 2-3 devices.

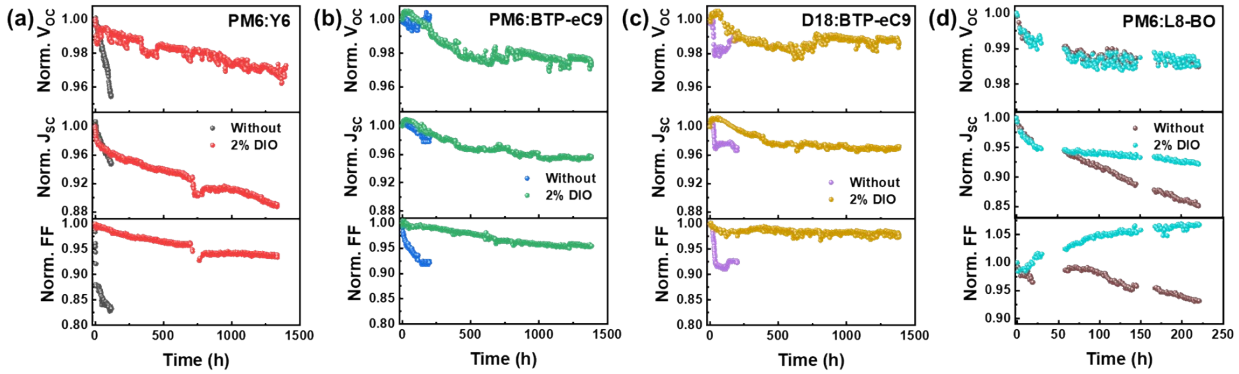

Fig. S32. The normalized photovoltaic parameters of a) PM6:Y6, b) PM6:BTP-eC9, c) D18:BTP-eC9 and d) PM6:L8-BO devices with PEDOT:F under white LED illumination.

Table S1. Photovoltaic parameters of inverted PHJ devices with different HTLs. The numbers in parentheses represent the average photovoltaic parameters (the average values for 5-10 devices) and their standard deviations.

	HTL	J_{SC} (mA/cm^2)	V_{OC} (V)	FF (%)	PCE (%)
Without DIO	MoO_3	6.40 (6.18±0.13)	0.863 (0.861±0.009)	69.91 (67.56±1.55)	3.86 (3.59±0.09)
	PEDOT: PSS	7.41 (7.23±0.11)	0.857 （0.858±0.005）	69.28 （67.98±0.59）	4.40 （4.21±0.08）
	PEDOT: F	7.40 (7.12±0.20)	0.869 （0.874±0.005）	68.76 （68.10±0.46）	4.42 （4.24±0.12）
2%DIO	MoO_3	9.02 (8.90±0.18)	0.844 （0.837±0.007）	77.39 （74.70±1.65）	5.89 （5.57±0.18）
	PEDOT: PSS	9.54 (8.71±0.71)	0.841 （0.834±0.004）	75.15 （74.83±0.58）	6.03 （5.43±0.45）
	PEDOT: F	10.28 （10.12±0.17）	0.847 （0.845±0.002）	76.11 （75.70±0.89）	6.63 （6.47±0.13）

Table S2. Statistics of integral J_{SC} of the PHJ device with different HTL before and after photo aging.

HTL	DIO		Integral J_{SC} (mA/cm^2)
MoO_3	0%	Fresh	6.07±0.38
		Aged	5.44±0.32
	2%	Fresh	8.64±0.02
		Aged	7.92±0.04
PEDOT: PSS	0%	Fresh	7.30±0.07
		Aged	6.17±0.06
	2%	Fresh	9.35±0.02
		Aged	8.88±0.07
PEDOT: F	0%	Fresh	7.50±0.01
		Aged	6.84±0.02
	2%	Fresh	10.23±0.15
		Aged	10.09±0.21

Table S3. The evolution of charge collection efficiency (P_{coll}) of the PHJ device with different HTL before and after photo aging.

HTL	DIO		P_{coll} (%)
MoO_3	0%	Fresh	72.80±0.14
		Aged	61.35±0.78
	2%	Fresh	84.95±0.07
		Aged	80.15±0.49
PEDOT: PSS	0%	Fresh	80.45±1.20
		Aged	59.70±0.57
	2%	Fresh	84.65±0.07
		Aged	76.55±1.48
PEDOT: F	0%	Fresh	74.90±2.69
		Aged	72.45±0.49
	2%	Fresh	85.05±0.35
		Aged	81.55±0.07

Table S4. The change of ideality factor n of the PHJ device with different HTL before and after photo aging.

HTL	DIO		n (kT/q)
MoO_3	0%	Fresh	1.06±0.01
		Aged	1.50±0.02
	2%	Fresh	1.36±0.02
		Aged	1.35±0.03
PEDOT: PSS	0%	Fresh	1.13±0.06
		Aged	1.33±0.01
	2%	Fresh	1.30±0.04
		Aged	1.28±0.04
PEDOT: F	0%	Fresh	1.01±0.01
		Aged	1.09±0.02
	2%	Fresh	1.01±0.02
		Aged	1.03±0.08

Table S5. The energy loss (E_{loss}) of different PHJ devices before and after photo aging. $\Delta E_1+\Delta E_2$ is the energy between optical bandgap with the radiative voltage limit times elementary charge; ΔE_3 is the non-radiative voltage losses times elementary charge; E_{loss} is the total voltage losses times elementary charge

HTL	DIO		$\Delta E_1+\Delta E_2$ (eV)	ΔE_3 (eV)	E_{loss} (eV)
MoO_3	0%	Fresh	0.307±0.001	0.206±0.002	0.513±0.003
		Aged	0.306±0.001	0.222±0.002	0.528±0.003
	2%	Fresh	0.306±0.001	0.232±0.002	0.538±0.004
		Aged	0.315±0.002	0.222±0.001	0.537±0.003
PEDOT: PSS	0%	Fresh	0.316±0.001	0.215±0.003	0.531±0.004
		Aged	0.316±0.001	0.239±0.003	0.556±0.003
	2%	Fresh	0.318±0.001	0.241±0.001	0.559±0.001
		Aged	0.318±0.001	0.241±0.003	0.559±0.001
PEDOT: F	0%	Fresh	0.338±0.001	0.187±0.005	0.525±0.001
		Aged	0.315±0.001	0.214±0.003	0.529±0.0.002
	2%	Fresh	0.358±0.001	0.190±0.001	0.548±0.006
		Aged	0.310±0.001	0.242±0.003	0.552±0.002

Table S6. Peak fit parameters including chemical assignment, peak position, full-width half-max, and area percentage for XPS regional spectra of pure PM6 and MoO_3 films.

XPS Peak Fits		PM6			MoO_3		
Orbital	Assignment	BE (eV)	FWHM (eV)	Area (%)	BE (eV)	FWHM (eV)	Area (%)
Carbon 1s	C-C	284.4	0.97	68.7			
	C-O	284.9	0.88	24.6			
	C_{crux}	286.6	0.88	5.5			
	C=O	288.0	0.88	1.1			
Oxygen 1s	C=O, $O_{lattice}$	530.6	1.11	26.9	530.6	1.25	75.4
	$C=O_{alkyl}$	531.8	1.11	67.1			
	$O_{vacancy}$				532.0	1.82	24.6
	shake	535.34	1.11	6.0			
Sulfur 2p	S-C 3/2	163.6	0.80	64.0			
	S-C 1/2	164.8	0.80	36.0			
Molybdenum 3d	Mo=O 5/2				232.7	1.06	62.5
	Mo=O 3/2				235.9	1.09	37.5

Table S7. Peak fit parameters including chemical assignment, peak position, full-width half-max, and area percentage for XPS regional spectra of PM6 (transfer printing)/MoO_3 films before and after photo aging.

XPS Peak Fits		Fresh			Aged		
Orbital	Assignment	BE (eV)	FWHM (eV)	Area (%)	BE (eV)	FWHM (eV)	Area (%)
Carbon 1s	C-C	284.3	1.13	86.5	284.5	1.11	72.4
	C-O	284.8	1.28	1.9	285.2	1.11	2.0
	C_{crux}	286.2	1.28	10.8	286.3	1.11	10.7
	C=O	287.6	1.28	0.7	287.5	1.11	3.0
	C(=O)O				288.7	1.11	2.0
Oxygen 1s	C=O, Mo=O, S=O	530.6	1.28	60.7	530.5	1.17	46.3
	$C=O_{alkyl}$	531.7	1.28	39.2	531.5	1.17	17.4
	$C\text{-}OH_{alkyl}$				532.0	1.17	23.5
	$C\text{-}O\text{-}C_{alkyl}$				532.9	1.17	12.9
Sulfur 2p	S-C 3/2	163.5	0.87	62.6	163.7	0.84	46.9
	S-C 1/2	164.6	0.87	37.4	163.9	0.84	12.8
	S-C-C=O 3/2				164.9	0.84	22.3
	S-C-C=O 1/2				165.7	0.84	22.4
	S=O 3/2				167.9	1.41	8.6
	S=O 1/2				169.0	1.41	7.2

Table S8. Peak fit parameters including chemical assignment, peak position, full-width half-max, and area percentage for XPS regional spectra of PM6:MoO_3 blend films before and after photo aging.

XPS Peak Fits		Fresh			Aged		
Orbital	Assignment	BE (eV)	FWHM (eV)	Area (%)	BE (eV)	FWHM (eV)	Area (%)
Carbon 1s	C-C	284.3	1.18	69.0	284.6	1.20	71.9
	C-O	284.7	1.53	5.0	284.9	1.20	7.3
	C_{crux}	286.0	1.53	23.8	286.1	1.20	12.6
	C=O	288.1	1.53	2.2	287.3	1.20	3.5
	C(=O)O				288.8	1.20	4.7
Oxygen 1s	C=O, Mo=O, S=O	530.6	1.36	79.4	530.5	1.22	51.4
	$C=O_{alkyl}$	532.1	1.36	20.6	531.0	1.22	20.9
	$C\text{-}OH_{alkyl}$				531.8	1.22	17.4
	$C\text{-}O\text{-}C_{alkyl}$				532.8	1.22	10.4
Sulfur 2p	S-C 3/2	163.4	0.89	66.0	163.6	0.86	31.9
	S-C 1/2	164.6	0.89	34.0	163.8	0.86	15.7
	S-C-C=O 3/2				164.8	0.86	16.6
	S-C-C=O 1/2				165.2	0.86	8.0
	S=O 3/2				168.1	1.90	18.1
	S=O 1/2				169.5	1.90	9.7

Table S9. Detailed GIWAXS (010) peak information in OOP of different films.

	Out-of-plane (010)				
	Angle (°)	Location ($Å^{-1}$)	d-spacing (Å)	FWHM ($Å^{-1}$)	CCL (Å)
Y6/PM6-Without	0.08	1.616	3.89	0.319	17.72
	0.09	1.612	3.90	0.325	17.39
	0.10	1.612	3.90	0.312	18.12
	0.11	1.613	3.89	0.298	18.97
	0.12	1.615	3.89	0.300	18.84
	0.13	1.605	3.91	0.313	18.06
	0.14	1.609	3.90	0.313	18.06
Y6/PM6-2%DIO	0.08	1.623	3.87	0.271	20.86
	0.09	1.619	3.88	0.258	21.91
	0.10	1.618	3.88	0.274	20.63
	0.11	1.616	3.89	0.251	22.52
	0.12	1.608	3.91	0.262	21.57
	0.13	1.575	3.99	0.195	28.98
	0.14	1.600	3.93	0.262	21.57

Table S10. Fitting parameters of 1D GISAXS profiles of Y6/PM6 films at different incident angles.

	Angle (°)	ξ (nm)	η (nm)	D	$2R_g$ (nm)
Y6/PM6-Without	0.08	24.5	7.0	3.0	34.4
	0.09	19.4	6.4	3.0	31.2
	0.10	18.7	6.8	3.0	33.2
	0.11	17.7	7.1	3.0	34.6
	0.12	18.8	7.2	3.0	35.2
	0.13	17.3	6.9	3.0	33.6
	0.14	17.9	7.0	3.0	34.2
Y6/PM6-2%DIO	0.08	17.6	7.6	3.0	37.0
	0.09	16.6	7.8	3.0	38.2
	0.10	16.4	7.5	3.0	36.8
	0.11	15.8	7.5	3.0	36.8
	0.12	15.7	7.4	3.0	36.2
	0.13	15.5	7.2	3.0	35.0
	0.14	15.2	7.0	3.0	34.4

Table S11. Photovoltaic parameters of inverted BHJ devices with different HTL. The numbers in parentheses represent the average photovoltaic parameters (the average values for 5-10 devices) and their standard deviations.

		HTL	J_{SC} (mA/cm^2)	V_{OC} (V)	FF (%)	PCE (%)
PM6:Y6	Without DIO	MoO_3	25.66 (25.65±0.30)	0.813 (0.811±0.002)	71.59 (69.77±1.60)	14.94 (14.52±0.30)
		PEDOT: PSS	24.69 (24.45±0.25)	0.817 (0.810±0.006)	67.95 (67.41±0.53)	13.70 (13.36±0.28)
		PEDOT: F	27.03 (27.00±0.16)	0.823 (0.822±0.001)	69.50 (69.12±0.43)	15.46 (15.33±0.11)
	2%DIO	MoO_3	23.96 (23.66±0.48)	0.765 (0.764±0.004)	69.15 (68.65±0.49)	12.68 (12.42±0.29)
		PEDOT: PSS	24.03 (23.98±0.08)	0.725 (0.723±0.003)	67.21 (66.35±0.72)	11.70 (11.51±0.19)
		PEDOT: F	26.04 (25.89±0.23)	0.721 (0.717±0.003)	68.62 (68.33±0.43)	12.88 (12.69±0.18)
PM6: BTP-eC9	Without	MoO_3	24.82 (25.13±1.44)	0.779 (0.778±0.008)	70.34 (65.18±3.67)	13.60 (12.72±0.79)
		PEDOT: PSS	25.54 (23.36±1.68)	0.746 (0.737±0.020)	61.99 (60.86±2.95)	11.82 (10.48±1.01)
		PEDOT: F	26.04 (25.09±0.88)	0.801 (0.787±0.008)	71.95 (71.33±1.16)	15.01 (14.09±0.60)
	0.5%DIO	MoO_3	23.75 (22.24±1.12)	0.713 (0.708±0.011)	67.83 (67.18±2.37)	11.49 (10.58±0.68)
		PEDOT: PSS	24.45 (25.35±2.01)	0.760 (0.745±0.021)	63.32 (57.17±7.63)	11.77 (10.72±0.94)
		PEDOT: F	26.61 (26.31±1.28)	0.784 (0.785±0.003)	64.51 (62.15±4.07)	13.45 (12.81±0.32)
D18: BTP-eC9	Without	MoO_3	24.44 (24.23±1.03)	0.805 (0.806±0.012)	67.83 (62.46±4.17)	13.34 (12.18±0.75)
		PEDOT: PSS	21.75 (21.85±0.18)	0.732 (0.720±0.009)	69.79 (68.67±2.18)	11.11 (10.80±0.39)
		PEDOT: F	24.67 (24.28±0.43)	0.840 (0.827±0.006)	72.23 (71.38±1.78)	14.96 (14.33±0.49)
	0.5%DIO	MoO_3	22.78 (21.88±1.10)	0.761 (0.762±0.017)	62.30 (61.80±4.44)	10.81 (10.28±0.60)
		PEDOT: PSS	26.19 (24.16±1.38)	0.760 (0.749±0.020)	67.89 (68.92±1.99)	13.52 (12.47±0.71)
		PEDOT: F	23.80 (21.75±1.90)	0.825 (0.823±0.007)	70.92 (69.95±2.74)	13.92 (12.50±0.85)
PM6:L8-BO	Without	PEDOT: F	25.82 (25.79±0.31)	0.887 (0.886±0.003)	71.70 (69.43±1.23)	16.43 (15.88±0.39)

	0.5%DIO		26.66 （26.28±0.32）	0.871 （0.868±0.005）	74.55 （73.17±1.29）	17.32 （16.61±0.36）

Table S12. Fitting parameters of 1D GISAXS profiles of BHJ films at different incident angles.

	Angle (°)	ξ (nm)	η (nm)	D	$2R_g$ (nm)
PM6:Y6	0.08	22.7	2.3	3.0	11.4
	0.16	23.6	4.2	3.0	20.4
	0.20	22.7	3.4	3.0	16.8
PM6:Y6 (2%DIO)	0.08	34.0	4.7	3.0	23.0
	0.16	39.2	5.3	3.0	25.9
	0.20	40.3	5.0	3.0	24.5
PM6: BTP-eC9	0.08	55.0	4.6	3.0	22.5
	0.16	53.1	4.8	3.0	23.5
	0.20	43.5	4.8	3.0	23.5
PM6: BTP-eC9 (0.5%DIO)	0.08	25.8	9.4	3.0	46.1
	0.16	26.7	9.9	3.0	48.5
	0.20	29.0	8.7	3.0	42.6
D18: BTP-eC9	0.08	18.5	3.2	3.0	15.8
	0.16	19.1	2.0	3.0	9.6
	0.20	20.5	3.3	3.0	16.0
D18: BTP-eC9 (0.5%DIO)	0.08	25.4	8.6	3.0	42.2
	0.16	23.7	8.4	3.0	41.2
	0.20	40.0	9.2	3.0	45.1
PM6: L8-BO	0.08	31.1	4.8	3.0	23.5
	0.16	45.9	7.1	3.0	34.8
	0.20	31.6	6.7	3.0	32.8
PM6: L8-BO (0.5%DIO)	0.08	32.8	5.7	3.0	27.9
	0.16	43.1	7.7	3.0	37.7
	0.20	39.7	7.3	3.0	35.8

Table S13. Detailed GIWAXS (010) peak information in OOP of different BHJ films.

	Out-of-plane (010)				
	Angle (°)	Location ($Å^{-1}$)	d-spacing (Å)	FWHM ($Å^{-1}$)	CCL (Å)
PM6:Y6	0.08	1.645	3.82	0.407	13.89
	0.16	1.630	3.85	0.326	17.33
	0.20	1.616	3.89	0.372	15.19
PM6:Y6 (2%DIO)	0.08	1.729	3.62	0.120	41.10
	0.16	1.607	3.91	0.259	21.82
	0.20	1.6020	3.88	0.260	21.68
PM6: BTP-eC9	0.08	1.597	3.93	0.332	17.02
	0.16	1.613	3.89	0.254	22.25
	0.20	1.629	3.86	0.256	22.08
PM6: BTP-eC9 (0.5%DIO)	0.08	1.671	3.76	0.110	51.38
	0.16	1.668	3.76	0.112	50.46
	0.20	1.684	3.73	0.142	39.80
D18: BTP-eC9	0.08	1.695	3.71	0.299	18.90
	0.16	1.616	3.89	0.199	28.40
	0.20	1.630	3.85	0.205	27.57
D18: BTP-eC9 (0.5%DIO)	0.08	1.660	3.78	0.078	72.46
	0.16	1.666	3.77	0.077	73.40
	0.20	1.660	3.78	0.112	50.46
PM6: L8-BO	0.08	1.810	3.47	0.450	12.56
	0.16	1.787	3.51	0.406	13.92
	0.20	1.775	3.54	0.274	20.62
PM6: L8-BO (0.5%DIO)	0.08	1.691	3.71	0.403	14.02
	0.16	1.714	3.66	0.343	16.48
	0.20	1.740	3.61	0.326	17.34

References

1 Debye, P.; Anderson, H.R.; Brumberger, H. Scattering by an Inhomogeneous Solid .2. The Correlation Function and Its Application. *J Appl Phys*. **1957,** *28* (6), 679-683.

2 Griffith, W.L.; Triolo, R.; Compere, A.L. Analytical Scattering Function of a Polydisperse Percus-Yevick Fluid with Schulz-(Gamma-) Distributed Diameters. *Phys Rev A*. **1987,** *35* (5), 2200-2206.

3 Liao, H.C.; Tsao, C.S.; Shao, Y.T.; Chang, S.Y.; Huang, Y.C.; Chuang, C.M.; Lin, T.H.; Chen, C.Y.; Su, C.J.; Jeng, U.S.; Chen, Y.F.; Su, W.F. Bi-hierarchical Nanostructures of Donor-acceptor Copolymer and Fullerene for High Efficient Bulk Heterojunction Solar Cells. *Energ Environ. Sci*. **2013,** *6* (6), 1938-1948.

4 Rau, U.; Blank, B.; Müller, T.C.M.; Kirchartz, T. Efficiency Potential of Photovoltaic Materials and Devices Unveiled by Detailed-Balance Analysis. *Phys. Rev. Appl*. **2017,** *7* (4).

5 Wang, Y.M.; Qian, D.P.; Cui, Y.; Zhang, H.T.; Hou, J.H.; Vandewal, K.; Kirchartz, T.; Gao, F. Optical Gaps of Organic Solar Cells as a Reference for Comparing Voltage Losses. *Adv. Energy Mater*. **2018,** *8* (28).

6 Hohm, D.P.; Ropp, M.E. Comparative Study of Maximum Power Point Tracking Algorithms. *Prog Photovoltaics*. **2003,** *11* (1), 47-62.